Quantum well structures in thin metal films: simple model physics in reality?

2002 Rep. Prog. Phys. 65 99

(http://iopscience.iop.org/0034-4885/65/2/201)

INSTITUTE OF PHYSICS PUBLISHING REPORTS ON PROGRESS IN PHYSICS

Rep. Prog. Phys. **65** (2002) 99–141 PII: S0034-4885(02)12597-8

Quantum well structures in thin metal films: simple model physics in reality?

M Milun[1], **P Pervan**[1] **and D P Woodruff**[2]

[1] Institute of Physics, PO Box 304, 10000 Zagreb, Croatia
[2] Physics Department, University of Warwick, Coventry CV4 7AL, UK

Received 3 October 2001
Published 8 January 2002
Online at stacks.iop.org/RoPP/65/99

Abstract

The quantum wells formed by ultra-thin metallic films on appropriate metallic substrates provide a real example of the simple undergraduate physics problem in quantum mechanics of the 'particle in a box'. Photoemission provides a direct probe of the energy of the resulting quantized bound states. In this review the relationship of this simple model system to the real metallic quantum well (QW) is explored, including the way that the exact nature of the boundaries can be taken into account in a relative simple way through the 'phase accumulation model'. More detailed aspects of the photoemission probe of QW states are also discussed, notably of the physical processes governing the photon energy dependence of the cross sections, of the influence of temperature, and the processes governing the observed peak widths. These aspects are illustrated with the results of experiments and theoretical studies, especially for the model systems Ag on Fe(100), Ag on V(100) and Cu on fcc Co(100).

(Some figures in this article are in colour only in the electronic version)

Contents

1. Introduction

The most common way of first introducing students to some of the key implications of quantum mechanics is the 'particle in a box' problem. By localizing an electron in a one-dimensional square well with infinite walls and requiring a wave-like solution, or more formally by solving the time-independent Schrödinger equation, one obtains the result that localization in a well of atomic dimensions leads to discrete (quantized) energy states separated by energies of the order of electron volts. The first practical example of this energy quantization through localization which is usually introduced to students is that of the discrete electronic energy levels in atoms, and notably in the hydrogen atom; strictly, of course, the one-dimensional well is not a good model of the hydrogen atom because the relevant (Coulomb) potential is intrinsically three-dimensional in character, but the correct mathematical treatment of this situation is significantly more complicated.

In the last few years our ability to 'engineer' artificial structures of reduced dimensionality on an atomic scale using, for example, molecular or atomic beam epitaxy and scanning probe microscopies, has led to investigations of real systems which come closer and closer to the simplest idealized textbook examples, such as the 'particle in a box'. Perhaps one of the most elegant visual examples of this is the 'quantum corrals' created on metallic surfaces by rings of adsorbed atoms placed with atomic precision using a scanning tunnelling microscope (STM) to manipulate the atoms; STM then allows one to observe the electron standing waves associated with two-dimensional bound states within this circular potential wall. We will only touch on this type of experiment here, but refer the reader to [1] for a fuller discussion. Here we concern ourselves primarily with the one-dimensional potential wells formed by the deposition of ultra-thin layers of material A on material B. The earliest examples of such structures are in semiconductor materials, and indeed many practical semiconductor devices now exist which exploit the novel electronic properties of such structures. Examples of articles concerned with semiconductor heterostructures and their associated QWs can be found in [2]. More recently an increasing number of examples of metal-on-metal quantum well (QW) structures have been investigated, and it is these systems which form the basis of the present review. In principle, at least, the wells produced by the deposition of 'simple' metals on metal surfaces, and their investigation by angle-resolved photoemission, provide the simplest cases of one-dimensional wells and thus the real structures with properties closest to those of the examples of the student textbooks. There is also a practical interest in metallic QWs which is of especial relevance to ferromagnetic materials and appears to lie at the heart of the origins of so-called giant magnetoresistance. We will touch on this aspect only briefly, and refer the reader interested in more details to other reviews [3, 4] .

Historically, the first experimental observations of so-called quantum size effects (QSE) in thin metallic films go back to the 1970s when interference effects were observed in the reflection of low-energy electrons from thin gold films [5]. The effect was ascribed to the interference of electrons reflected at the substrate–film and vacuum–film interfaces and was observed for all thicknesses less than 100 Å. Within this model, and assuming a very small phase change (f) at the two interfaces separated by the thickness, L, the total phase change for a round trip back and forth through the film is given by $\vartheta = (4\pi L/\lambda) + f$. In agreement with this model, the interference period was found to decrease as the film thickness increased and the reflectivity maxima shifted to lower energies with increasing temperature, as may be expected due to the thermal expansion of the film thickness. Based on this simple theory, simulation of the data indicated that the kinetic energy gain of the electrons in entering the gold film from the vacuum (the inner potential) was 16 ± 1.6 eV, a value generally consistent with that obtained by other methods. This idea of standing wave formation due to the QSE

was pursued by Jaklevic [6, 7] to explain oscillations observed in electron tunnelling through thin metallic films of Mg, Pb, Au and Ag. The effect was observable up to a thickness of 500 Å. The interpretation of the data was unfortunately complicated by the fact that the film thickness could not be controlled very precisely; specifically, the films comprised regions of different thicknesses and the observed effects were dominated by the subset of states which have the same energy for all values of the thickness. For these electrons, having energies above the Fermi level, a lifetime of 10^{-23} s and a width of 25 meV was estimated, which gave a mean free path of 1000 Å. Later Jalochowski *et al* [8] extended tunnelling experiments to Pb/Ag sandwiched structures and observed two periods of oscillations. Further experimental work on the QSE exploring the reflectivity and transmission of electrons normally incident on epitaxially grown thin metallic films (of Cu and Ag on a W(110)) was performed by Jonker *et al* [9–11] and Park *et al* [12, 13] (for Cu/Ni(001), Ag/Cu(111), Ag/Si(111) and Cu/Si(111)), Zhu *et al* [14] and Zdyb *et al* [15].

All of this early work involved electrons above the Fermi level (and in some cases above the vacuum level) and thus probed only the standing wave states—the QW states—which are unoccupied. The first measurements providing evidence of occupied QW states were performed by measuring the electrical conductivity of Sn and In ultra-thin films during deposition [16] and the resistivity of Pt films in a wide range of thickness from 30–3000 Å [17]. Fischer *et al* [18–20] made an effort to produce clear experimental evidence for the existence of QSE in very thin Pt films. Chaudhari *et al* [21] explained their resistance measurements of gold films as a function of temperature and magnetic field in terms of the electron localization due to the QSE. Jalochowski *et al* [22–24] further documented the importance of the QSE in the resistivity measurements, this time using Pb films.

Once the existence of QW states and their importance for transport properties of thin metallic films was clearly established [25], a large number of different oscillatory phenomena in thin films have been explained within this picture. Probably the best known are phenomena such as the giant magnetoresistance found in certain magnetic multi-layered structures and superlattices mentioned above [3]. QSE in thin films have also been observed in helium atom scattering (HAS) experiments [26–29], in Hall effect measurements [30], in studies of second harmonic generation (SHG) [31, 32], work function measurements [33] and in the diamagnetic optical response of metallic (Ni, Al) ultra-thin films [34, 35]. Very recently it has also been shown that the electronic energy associated with the existence of QW states can play an important role in the stability of certain thicknesses of ultra-thin films [36].

By far the clearest and most direct information on the existence and energetics of quantized energy states localized in thin metallic films, however, comes from photoemission (and inverse photoemission); figure 1 shows an example of such experimental photoemission spectra. In this photoemission experiment [37] the number of electrons emitted perpendicular to the surface of thin epitaxial films of Ag grown on an Fe(100) substrate is plotted as a function of kinetic energy for a fixed photon energy of 16 eV. By convention, the kinetic energy scale is labelled in terms of the binding energy of the occupied electron states from which the electrons were emitted, effectively by subtracting the photon energy from the measured kinetic energy relative to the Fermi level of the solid, E_F. The binding energies are thus relative to E_F. Figure 1 shows distinct peaks associated with emission from the occupied QW states, and it is clear that, as the well becomes wider (the film become thicker), the energetic spacing of the allowed states becomes smaller, exactly as we would expect from the simple 'particle-in-a-box' model. In this particular case of very flat films discrete states are visible even for a film 119 monolayers (ML) thick, while in a true bulk solid these discrete states are replaced by a smooth continuum. This review is concerned with a detailed discussion of the theory and properties of these states and their investigation, principally by angle-resolved photoemission.

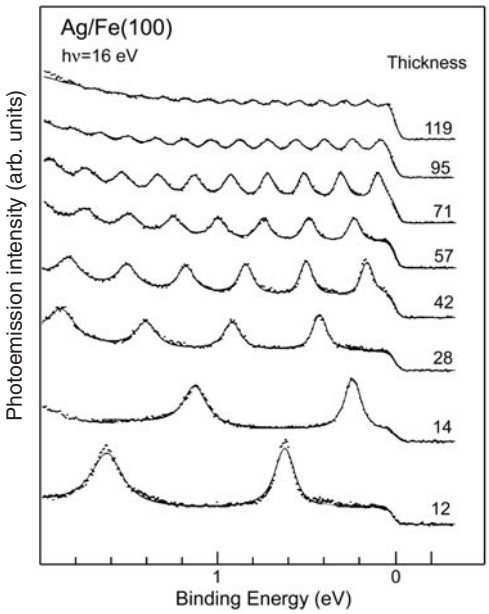

Figure 1. Photoemission spectra taken in a normal emission geometry for silver films of various thicknesses deposited on Fe(100) (adapted from [37, 41]).

The rest of this review is arranged as follows. Firstly, in section 2, we summarize the properties of the ideal rectangular one-dimensional well and show how these are reproduced in the case of metal-on-metal films. We compare the properties of ideal and real wells and introduce the primary experimental data on the QW energies derived from photoemission and inverse photoemission. We also compare the properties of these QW states with those of states localized at the clean surfaces of metals by the discontinuity of the crystalline periodic potential; because the real metallic QWs are not strictly rectangular in character, these surface states correspond to bound states of similar wells in which the film thickness goes to zero. In sections 3 and 4 we explore some more detailed aspects of the photoemission results, concerned with the physical processes which govern the relative intensities of photoemission at different photon energies from these QW states. In particular, section 3 addresses the role of the (crystalline) periodic potential in the substrate and within the film, while section 4 considers the special problems associated with the sharp changes in potential which occur at the well walls. Section 5 describes the influence of temperature changes on the energies of the QW states, while section 6 considers some of the factors which determine the spectral lineshapes of photoemission from these states including, in particular, the role of electron–phonon coupling. In section 7 we draw together some general conclusions.

2. One-dimensional quantum wells in metal-on-metal systems

2.1. Bound states in finite potential wells

Before considering any practical experiments it is useful to summarize briefly the results of the very simplest models. In the earliest undergraduate textbooks the starting point is generally of a particle in a one-dimensional box, taken to be represented by a one-dimensional well with infinite barriers. The key result is that the particle, which we will hereafter take to be an electron, must be represented by a standing wave having nodes at the walls of the well. Its associated wavelength is therefore given by

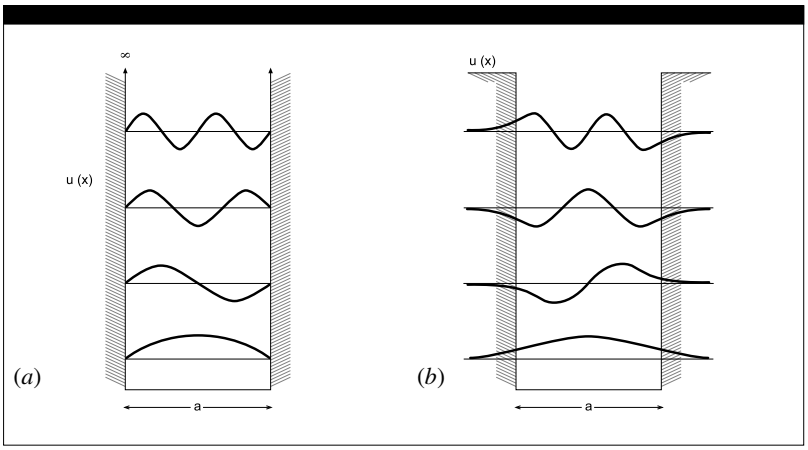

Figure 2. Schematic representations (not normalized) of the wavefunctions of the first few solutions for electron states in a one-dimensional square potential well, $U(x)$, of width a with *infinite* (a) and *finite* (b) walls.

$$\lambda_n = 2L/n \tag{1}$$

where L is the width of the well and n is an integer. From de Broglie's relationship relating the energy and wavelength of the electron one therefore finds the allowed (quantized) energies are

$$E_n = n^2 \frac{h^2}{8mL^2} \tag{2}$$

where m is the electron mass and h is Planck's constant. Figure 2(a) shows the associated wavefunctions for the lowest lying states. Notice that in this rectangular well the quantized energy levels have energy proportional to n^2, and thus become more widely spaced as the energy increases. By contrast, in the hydrogen atom, the fact that the potential walls are not square but involve a potential which falls off as $1/r$, where r is the radial distance from the nucleus, leads to quantized states with energies proportional to $1/n^2$, thus becoming more and more closely spaced with increasing n, leading to the Rydberg series which converges on the vacuum level.

A somewhat more realistic model of the particle-in-a-box problem is to take a rectangular well with finite potential walls. In this case the solutions are very similar to those of the infinite barrier well, but the wavefunctions at the well walls inside the well now match the exponential tails outside the well (see figure 2(b)). This problem can also be solved by the usual boundary conditions of matching both the amplitude and gradient of the wavefunctions inside and outside the well at the walls (in the infinite well case the wavefunction gradient is actually discontinuous at the wall due to the infinite barrier). The proper solution is already more complicated, but it is clear that the presence of the exponential tails on the wavefunctions leads to a slight increase in the wavelength relative to the infinite barrier case and thus a slight lowering of the energies.

A rather direct practical illustration of this problem, which has been observed using STM, is the case of electron states localized at metal surfaces which may also be constrained in their motion parallel to the surface by being trapped between two (single-atom height) atomic steps. Figure 3 shows an example of results from such an experiment [38]. The surface under study is Ag(111), which is known to show a surface-localized (Shockley) state which is free-electron-like in its movement parallel to the surface. The state is localized at the surface because it

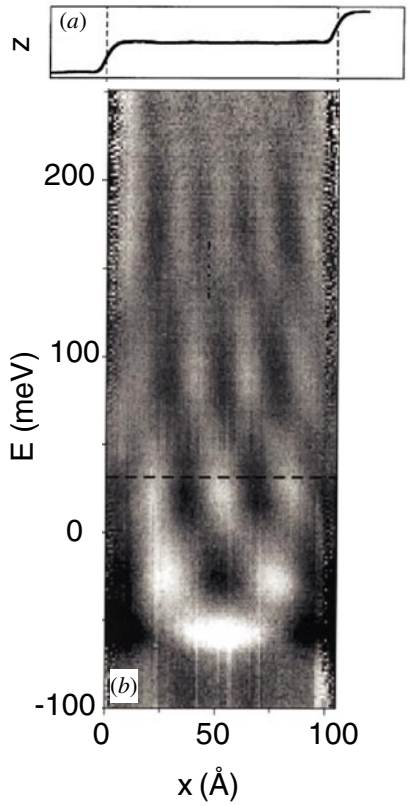

Figure 3. (*a*) STM constant-current line scan of the relative tip height above the surface over a 104 Å wide Ag(111) terrace confined by two single-atom-height steps that act as electron mirrors (broken lines). (*b*) Grey scale representation of the corresponding differential conductance as a function of sample–tip voltage showing the spatial variations in the electron density at different energies due to the confinement of the s–p surface state electrons [38].

has a binding energy which lies in a gap in the projection of the bulk band structure onto this surface. Two parallel surface steps then provide scattering barriers which effectively form a one-dimensional well. In STM one measures the electron current which tunnels through the vacuum gap between the surface and a fine conducting tip brought to within atomic dimensions of the surface. By varying the bias voltage between these, one detects changes in the current as the bias makes new bound states accessible for tunnelling, and the spatial variation of this change as one scans the tip along the line between the two steps provides a rather direct way of observing the spatial variation of the charge-density standing wave. At different bias voltages, corresponding to the bound state energies of these quantized energy states, one can map out the different charge densities. Figure 3 shows rather graphically that these variations are very similar to those predicted for the simple finite rectangular well of figure 2(*b*).

2.2. Quantum wells in ultra-thin metallic films

As remarked in the introduction, the central topic of this review is QWs created *perpendicular* to a surface in ultra-thin metallic films. In this case the spatial variation in the charge density associated with the discrete bound states of these wells lies within the film and cannot be observed in such a simple direct fashion as the lateral variations of constrained surface-localized states. There are also fundamental differences in the nature of the well walls which can lead to rather different bound state solutions. We now consider the fundamental aspects of metallic QWs of this type.

In the case of metallic films deposited on metal surfaces the nature of the two barriers which create the QW at the substrate/film interface and at the film/vacuum interface are quite

different. At the surface/vacuum interface, the barrier arises because we are concerned with bound states which lie between the bottom of the conduction band of the film and the vacuum level. If we bring an electron to a distance z from a metallic surface in the vacuum, the response of the metal is such as to create an image of the electron (but of opposite charge) a distance z below the surface, so the electron experiences a Coulombic attraction determined by the separation of the two charges, $2z$, creating a potential

$$V_{\text{image}} = -\frac{e^2}{4\pi\varepsilon_0 \cdot 4z} \tag{3}$$

where e is the electronic charge and ε_0 is the permittivity of free space. While this description is clearly not strictly appropriate as the distance z becomes of atomic dimensions, this image potential is usually regarded as an effective description of the vacuum barrier. At the film/substrate interface, on the other hand, an electron can only be confined in the film if its energy lies in a band gap of the substrate. Of course, a metal does not have a total gap in the occupied part of the conduction band; however, the electronic bands of a real metal depend on the direction, and the Fermi surface is far from spherical for many metals, so gaps do appear around the Fermi level in specific directions. Moreover, even in directions in which the metal does have band states around the Fermi level, the fact that these states have a well-defined symmetry may mean that there is a 'symmetry gap' relative to states in the film of a different symmetry which cannot then couple to the bulk states. In practice, there are many metal surfaces for which, relative to propagation perpendicular to the surface, the solid has a band gap (or a symmetry gap) which may have a width of a few eV and is centred within a few eV of the Fermi level. Under these circumstances an electron in the overlayer film moving perpendicular to the surface with an energy lying within the projected bulk gap cannot couple to any bulk states and will therefore be reflected at the film/substrate interface. The resulting potential barrier for such an overlayer film is illustrated schematically in figure 4.

In order to solve the Schrödinger equation for this situation we need to describe the electron potential in the substrate, because the wavefunction of any bound QW state in the film must match onto some decaying ('evanescent') wavefunction in this substrate, so the problem is now much more complicated than the situations we have discussed so far. To circumvent this, an alternative (and more physically transparent) way of solving the problem is usually used. In the so-called phase accumulation model [39, 40] (also referred to as the Bohr–Sommerfeld quantization rule [41]) one treats the problem as one of a travelling electron wave bouncing back and forth between the substrate/film and film/vacuum interface. If the round-trip phase accumulation associated with the propagation between the barriers and the phase shifts associated with the reflections is an integral multiple of 2π, then a standing wave solution corresponding to a bound state occurs. The simplification achieved by treating the problem in this way arises because one can describe the influence of the underlying substrate by a phase shift, ϕ_C, experienced at the substrate/film boundary which can be calculated from a simple two-band model of the substrate. The condition for a standing wave, and thus a quantized state of the well of width d, is

$$\phi_B + \phi_C + 2kd = 2\pi n \tag{4}$$

where k is the electron wavevector in the film perpendicular to the surface, $2kd$ is the phase accumulated in travelling back and forth in the film and ϕ_B is the phase shift on reflection at the film/vacuum interface. Notice, incidentally, that d is measured between the two interfaces, usually taken to be located at one half of an atomic layer spacing beyond the termination of the crystal substrate and the outermost atom layer of the film. The fact that the image potential barrier extends beyond this terminating plane is accounted for in the associated phase shift.

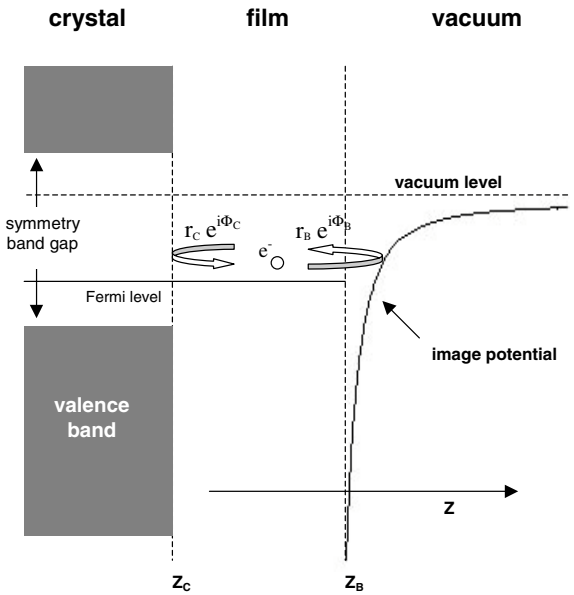

Figure 4. Schematic diagram showing the multiple reflection (phase accumulation) model used to describe the electron bound states in a thin film on a surface due to confinement between the image potential on the vacuum side and the crystal potential at an energy corresponding to a symmetry band gap in the substrate [45]. In the case of zero film thickness the lowest energy solution is a surface state and higher energy solutions are so-called image potential states. r_C and r_B are the reflection coefficients at the crystal and vacuum barriers, respectively.

A useful approximation for this phase shift is [42,43]

$$\phi_B/\pi = [3.4/(E_V - E)]^{1/2} - 1 \tag{5}$$

in which the energies of the vacuum level, E_V, and of the bound state of the electron, E, are expressed in eV. For a so-called Shockley-inverted band gap in the crystal substrate, the phase shift at the interface varies from $-\pi$ at the bottom of the band gap to 0 at the top (figure 5), and in a simple two-band nearly-free electron picture of the substrate one can write as an approximate and purely empirical formula

$$\phi_C = 2\arcsin[(E - E_L)/(E_U - E_L)]^{1/2} - \pi \tag{6}$$

where E_L and E_U are the energies of the lower and upper energies of the band gap. (Notice, incidentally, that the term 'Shockley inverted' is rather misleading; in such a band gap the state at the bottom of the gap is p-like, with charge accumulating between the atoms as expected for a bonding state, whereas at the top of the gap the state is s-like, with charge concentrated on the atoms and thus having anti-bonding character. The 'inversion' is relative to free atoms in which s-states generally have lower energies than p-states.) This simple multiple scattering model was actually first introduced by Echenique and Pendry [39] and later exploited especially by Smith and co-workers [44–46] in order to explain some features of the electronic structure of clean metal surfaces. Even if we set the overlayer film thickness equal to zero, the step wall at the crystal termination and the $1/z$ image potential create a well in which bound states can exist, and indeed, as in the case of the hydrogen atom, the $1/z$ long-range potential means that a Rydberg series of states, which have energies converging on the vacuum level, exists. These 'image potential' states for $n = 1, 2, 3, \ldots$, etc, are within 1–2 eV of the vacuum level and thus above the Fermi level and normally unoccupied, but they can be detected by probes

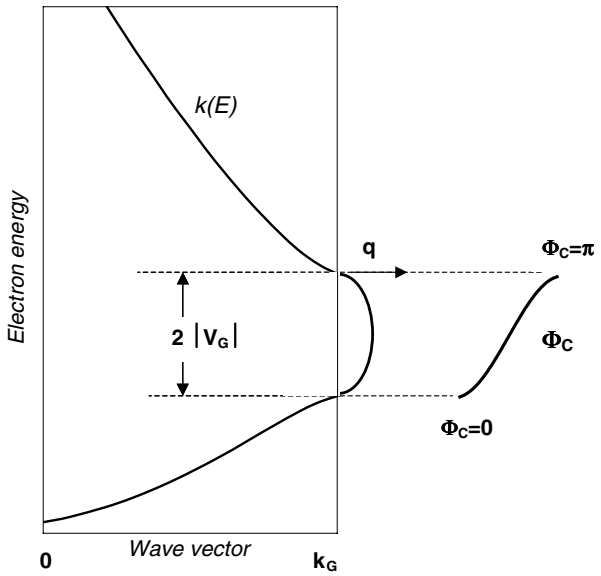

Figure 5. Schematic representation of a simple one-dimensional s–p band gap (left) and the associated phase change (right) in electrons reflected from this solid as a function of the energy within the gap. q is the imaginary part of the wavevector across the energy band gap.

of unoccupied states such as inverse photoemission and two-photon photoemission. Perhaps even more surprising is that the $n = 0$ solution of these equations corresponds to the intrinsic (Shockley) surface state at the surface which, despite the crude character of the model for a clean surface, is typically predicted to occur with a binding energy within 0.1–0.2 eV of its observed value.

To illustrate the basic systematics which emerge from the application of this theory of QW states in ultra-thin metallic films we show some of our own results for films of Ag on a V(100) surface [47] together with spectra from Ag films on Fe(100) in the same thickness range [48]. Notice that the spectrum for 3 ML of Ag on V(100) is omitted because no QW state occurs within the V(100) band gap for this film thickness. Figure 6 shows the actual photoelectron energy spectra, while figure 7 shows a set of graphical solutions using the phase accumulation model which predict the QW state energies for both of these substrate/overlayer systems, but also for the system fcc Co(100)/Cu which we discuss below. In each of these graphs the dotted curves show the energy dependence of the $2kNa$ component of the phase for different film thicknesses (N ML) while the full curves show the sum $2\pi n - (\phi_B + \phi_C)$. The crossing points of these curves correspond to the predicted QW state energies, and are joined by broken curves having the same value of $n - N$ (see below). The photoemission spectra of figure 6, recorded in normal emission and thus corresponding to the QW states with no component of k parallel to the surface, show clear intense peaks associated with the occupied QW bound states, while figure 7 shows that the predicted energies agree quite well with the observations. The photoemission spectra of figure 6 show a superficially rather complex behaviour of the binding energy of the QW states with overlayer film thickness; for example, the binding energy falls from 1 to 3 ML, increases at 4 ML and then falls again from 4 to 6 ML, and so on. To understand this, it is helpful to consider briefly the physical constraints of the situation. Notice, in particular, that in the limit of a simple square-well potential the quantized energy states for wells which are only a few atomic spacings wide are quite widely spaced, and that the energy band gap of the substrate in which these states exist is quite narrow. All allowed QW states

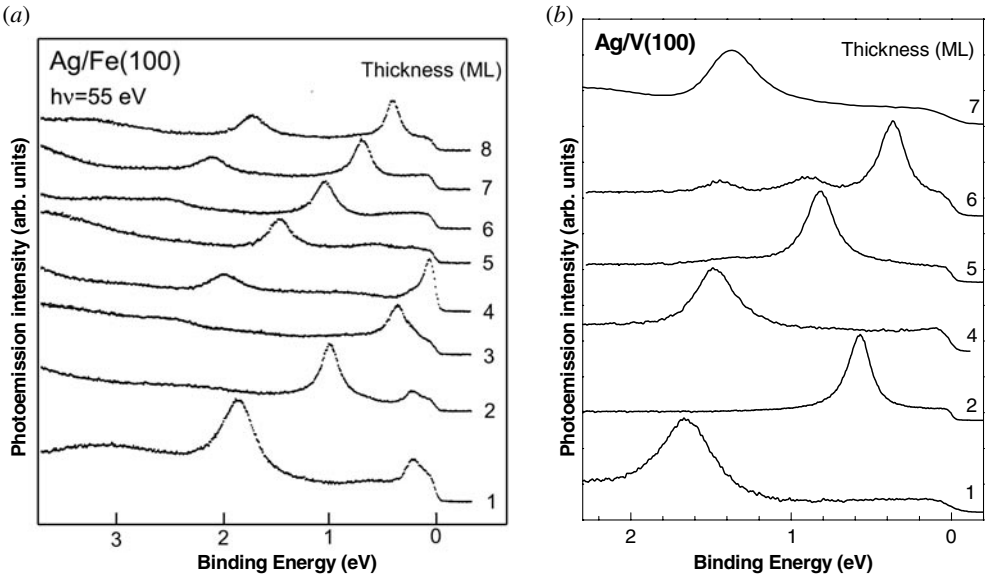

Figure 6. Normal emission photoelectron energy spectra from ultra-thin silver films on (*a*) Fe(100) (adapted from [48]) and (*b*) V(100) (adapted from [47]).

must therefore have quite similar energies (within a range of 2 eV or so for occupied states) and so have similar wavelengths. Indeed, bearing in mind that the states lie in the lowest energy band gap of the substrate conduction band when the electron wavevector perpendicular to the surface is at the Brillouin zone boundary, and that the atomic layer spacing in the overlayer film is inevitably similar to that of the substrate (most metallic atoms have similar effective radii), it is clear that the wavelength of the electrons in the QW states will equal approximately twice the monolayer spacing for all film thicknesses.

This means that it is helpful to categorize the QW states not according to the number of nodes in the wavefunction within the film perpendicular to the surface (which equals n), nor according to the number of atomic layers in the film, N, but according to the *difference* between these two numbers, $\nu = N - n$ (see figure 7). We might then expect that all states with the same value of ν (and especially all states with $\nu = 1$) will have very similar energies. More careful inspection of figure 7, however, shows that, even for the states with $\nu = 1$, there will be a small change in the energy as the film thickness changes because of the role of the wavefunction tails outside the well. These tails cause the wavelength to increase and the energy to fall relative to the infinite barrier case for any particular well width, but this effect has less and less influence on the wavelength as the film thickness increases. The systematic trend is thus for QW states with the same value of ν to increase in energy (decrease in binding energy) as the film thickness increases. When this energy exceeds the Fermi energy, E_F, no thicker film can sustain an occupied QW state with this value of ν. However, states with a value of ν greater than unity can occur for slightly thicker films. This trend is clearly seen in figures 6 and 7.

An especially attractive illustration of this effect is seen in an elegant experiment of Kawakami *et al* [49] who constructed a wedge-shaped Cu film grown on an epitaxial fcc Co(100) surface. By scanning the incident photon beam over the film along the direction of increasing thickness and plotting the intensity of the photoemission spectrum on a grey scale (figure 8), one obtains a very direct experimental illustration of the predicted behaviour seen in figure 7. The numbers overlaid on the data at the top of the panel are the values of the

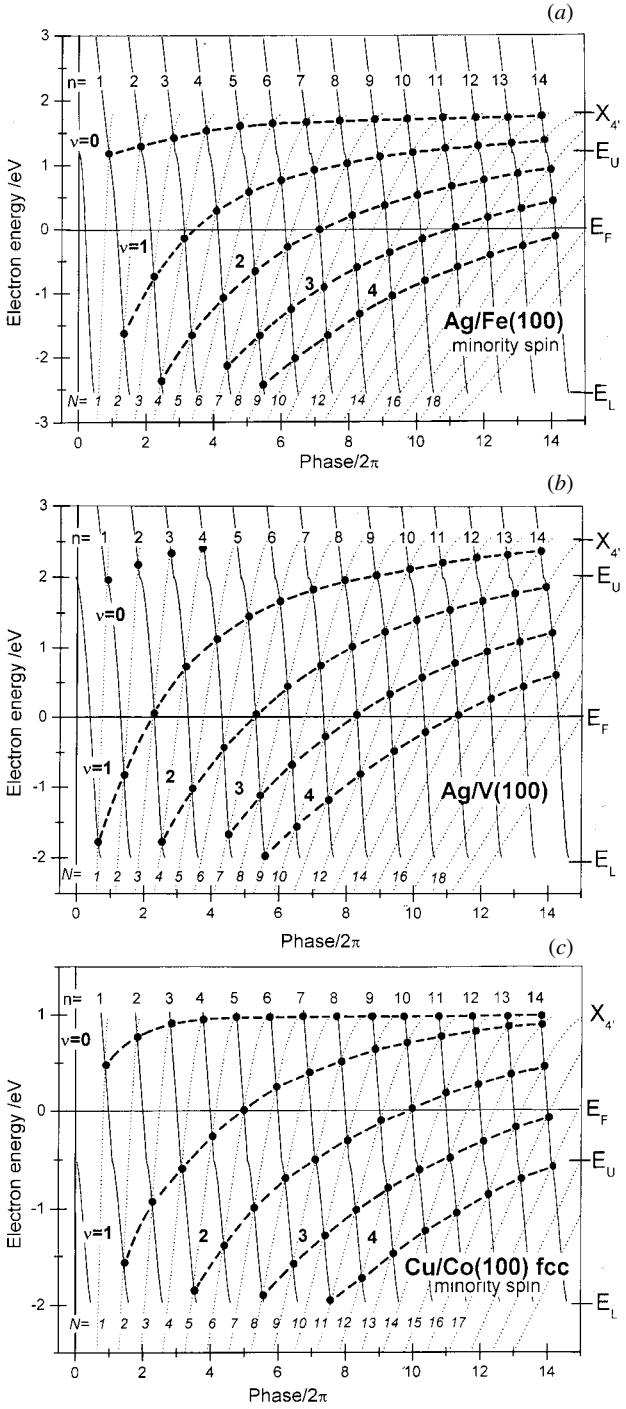

Figure 7. Graphical solutions for the QW state energies obtained from the phase accumulation model for the (*a*) Ag/Fe(100), (*b*) Ag/V(100) and (*c*) Cu/Co(100) fcc systems. For an explanation see the text.

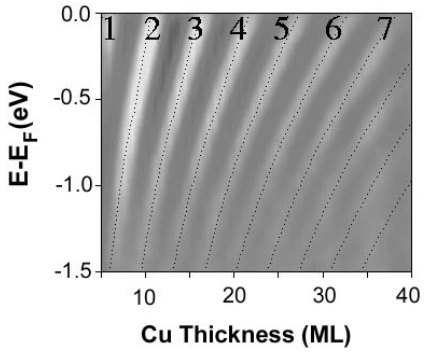

Figure 8. Half-tone map of the intensity of photoemission as a function of initial-state energy and copper film thickness on an fcc Co(111) substrate grown epitaxially on Cu(111). Cuts through this map parallel to the ordinate are photoelectron energy spectra, while the variation in film thickness represented by cuts parallel to the abscissa were obtained by scanning across a Cu film wedge [49].

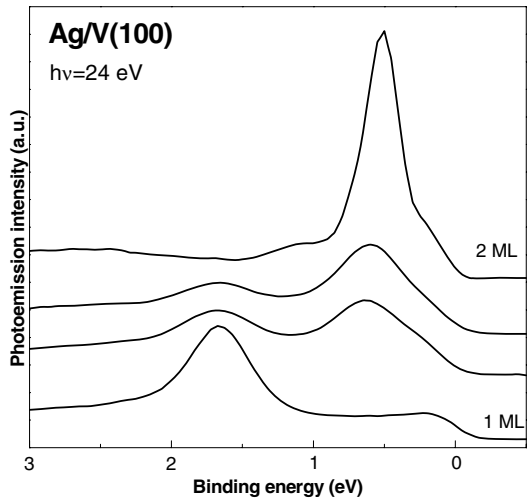

Figure 9. Normal emission photoelectron energy spectra from several silver films with thicknesses in the range 1–2 ML on V(100). Only two discrete QW state peaks are seen, which correspond to the states from 1 and 2 ML films. The films having an average thickness which corresponds to a non-integer number of atomic layers evidently comprise patches of both 1 and 2 ML films [47].

parameter ν. Notice, however, that comparison of the data of figure 8 with those of figure 6 highlights an important issue. In figure 6 QW states are only seen (and in figure 7 are only predicted) for discrete film thicknesses corresponding to integral numbers of atomic layers; for intermediate thicknesses in the V(100)/Ag and Fe(100)/Ag systems, one sees discrete peaks associated with each of the regions of the surface having a different discrete thickness, as for example with a coverage on V(100) of between 1–2 ML when the states associated with these two different coverages are seen (figure 9). Although figure 7 shows that these experimentally observed QW energies lie on a smoothly varying curve, the actual states are only seen at distinct film thicknesses (quantized by number of atomic layers). By contrast, the results from the Co(100)/Cu wedge appear to show continuously varying energy, apparently implying QW states associated with non-integral numbers of atomic layers. Notice, however, that figure 8 excludes data from the thinnest films (less than about 4–5 ML) for which the QW states are not clearly resolved in the full data set [49]. This epitaxial growth system is

known to produce relatively atomically rough surfaces, so the films actually comprise a narrow range of thicknesses in terms of atomic layers. For the thicker films, each film has a QW state with a similar energy, so the observed photoemission spectrum shows a relatively broad peak which comprises an envelope of several such peaks, and it is this envelope which is mapped in figure 8. In this regard the data shown earlier in figure 1 for quite thick (up to 110 ML) films of Ag on Fe(100) appear quite different. In this case the growth is evidently of an ideal layer-by-layer form even for such thick films, and the QW photoemission spectra indicate that the films are atomically flat at each stage in the growth.

While the phase-accumulation model is clearly very successful in describing the systematics of QW state energies in these metallic thin films, and the main trends can clearly be related to those of the finite-wall square potential well problem described in the previous section, it is interesting to compare the spatial distribution of the wavefunctions and associated charge density implied by these models. In order to do this, we need to relate the concept of the phase shift in the reflections at the well boundaries to the resulting form of the wavefunctions. Two extremes are especially simple to understand, because they have extremely simple classical wave analogues. The first of these is the situation seen in the infinite-wall well problem of figure 2(*a*) which places nodes at the walls. This is the analogue of the standing waves on a plucked string, and one needs a phase shift of π to ensure that the incident and reflected travelling waves exactly cancel at the boundary. The second extreme is the case of zero phase shift on reflection, which places an antinode at the boundary, equivalent to the case of a string with a loose end. Clearly the solutions seen in figure 2(*b*) for the finite-wall well correspond to an intermediate phase shift at the reflecting wall, leaving a finite value of the wavefunction at the wall which matches to the exponential tail outside the well. Small tails correspond to phase shifts close to π, while the extreme case of a phase shift close to 0 means that the wavefunction tail extends with far greater intensity, having an antinode only just inside the well (if the wavefunction were to be rising as it approached the wall from inside the well it could not match an exponential outside the well and no solution is possible).

In order to understand the full implications of the reflection phase shifts and the expected systematics of the QW state energies, it is helpful to consider some simple model cases and to then look at the results for a specific system, for which we take V(100)/Ag. Before considering specific models, however, we should note that the film thickness will be an integral number, N, of atomic layer thicknesses, a (apart from subtle relaxation effects), so one can recast equation (4) as

$$\phi_B + \phi_C + 2k \cdot Na = 2\pi n. \tag{7}$$

Consider now, the special case of $\phi_C = \phi_B = -\pi$. A phase shift of $\pm\pi$ leads to solutions with zero amplitude at the boundaries as for the infinite barrier well of figure 2(*a*). (Notice that, although this condition does correspond to the infinite well of figure 2(*a*), the associated equation (2) leads to a quantum number n which is one larger than that defined by the phase accumulation model of equation (7) due to the explicit inclusion here of the barrier phase shifts.) In this case, one of the solutions for *all* well widths has the same value of the electron wavevector, $k = \pi/a$ (see figure 10—top left panel) and thus the same energy; these states correspond to the combinations of parameters of $N = 1, n = 0$; $N = 2, n = 1$; $N = 3, n = 2$, etc, or more generally $N - n = 1$. This simple relationship highlights the value of defining the additional 'quantum number' $\nu = N - n$, mentioned above. For comparison we can evaluate the extreme opposite situation of $\phi_C = \phi_B \approx 0$ (notice that if the phase shifts are identically zero no solution is possible because the exponentially damped wavefunction outside the well cannot match in gradient at the boundary). In this case there is no solution for $n = 0$ (the only allowed value of the electron wavevector is zero) but a new set of states with $k = \pi/a$

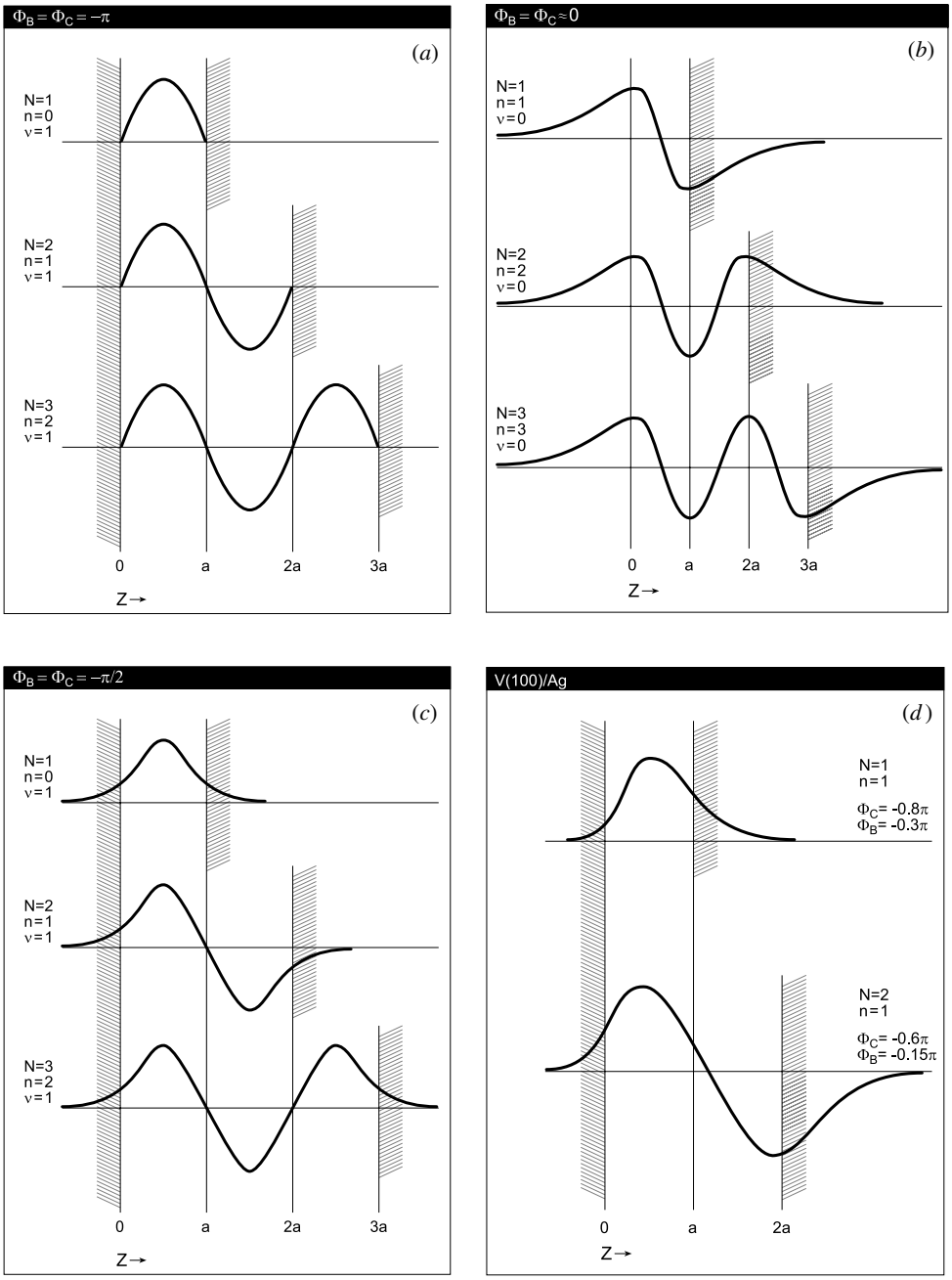

Figure 10. Sketches of the wavefunctions of QW states in square potential wells of widths a, $2a$ and $3a$ simulating the effects of one, two and there atomic layers. In (a) the potential wells have infinite height and so are the standard 'particle-in-a-box' solutions. The sketches in (b) show QW states confined between a symmetry band gap and the image potential for the case of both phase changes at the interface (ϕ_C) and vacuum side (ϕ_B) being close to zero, while in (c) is shown the result when these two phase shifts have the intermediate value of $\pi/2$. (d) Shows the spatial distribution of the wavefunctions given by equation (7) for the QW states seen in figure 6 for the thinnest films of Ag on V(100), using the actual phase shifts given by equations (5) and (6). Note that none of these sketched solutions take any account of the periodic potential of either the substrate or the thin film.

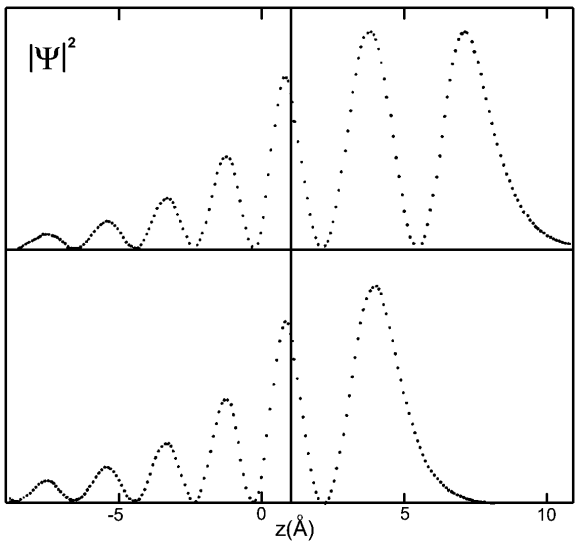

Figure 11. Charge distribution of QW states of 1 ML (lower panel) and 2 ML (upper panel) Na films on Cu(111) substrate as obtained from a tight-binding calculation, adapted from [50]. Negative values of z correspond to the substrate, with the film/substrate interface at $z = 0$. For both films the antinode furthest to the right lies just below the film/vacuum interface.

arise which correspond to $\nu = 0$. As may be seen from the sketches of figure 10, these states *inside* the well are just like the $\nu = 1$, $\phi_C = \phi_B = -\pi$ states described above, but shifted in phase within the well by $a/2$. Notice, however, that the energy correspondence between states with the different barrier phase shifts is with states associated with the same film thickness, but different n and ν values. Also sketched in figure 10 is the situation for the specific intermediate case of $\phi_C = \phi_B = -\pi/2$. Here the fact that the harmonic functions inside the wells must match the exponential tails outside the wells at points intermediate between the nodes and the antinodes has the effect of extending the wavelength and lowering the energies relative to the $\phi_C = \phi_B = -\pi$ case in a fashion similar to that seen in figure 2 comparing the infinite and finite wall square wells. Indeed, the k values for these states for 1, 2 and 3 ML film thickness are given by equation (7) in units of π/a as $1/2$, $3/4$ and $5/6$, respectively. This trend of increasing k and thus increasing energy with increasing film thickness for a specified value of ν is exactly what is seen in the data of figures 6 and 8. Finally, in figure 10 are included sketches of the spatial distribution of the wavefunctions given by equation (7) for the QW states seen in figure 6 for the thinnest films of Ag on V(100), using the actual phase shifts given by equations (5) and (6). One clear conclusion from these sketches is that the quantum number n corresponds to the number of nodal planes in the QW state wavefunction perpendicular to the surface, and this corresponds directly with the simple particle-in-a-box problem of figure 2.

It is important to add one caveat to the sketches of the QW state wavefunctions of figure 10 which are constructed on the basis of the solution *inside* the well from the phase accumulation model. Outside the well they are matched by exponentially decaying tails, but in reality the wavefunction in the near-surface region of the crystal substrate will not only be damped, but will also oscillate with a wavelength defined by the reciprocal lattice vector associated with the band gap of the substrate. An example of this is seen in figure 11; here the modulus squared of the wavefunctions of QW states for 1 and 2 ML of Na on Cu(111), calculated using a tight-binding formalism, is shown [50]. Although there are no solutions to the Schrödinger

equation for electrons in the band gap within an infinite periodic crystal, solutions with complex wavevectors are allowed at defects such as a surface; the real part of the wavevector is then fixed across the gap, but the imaginary part, which determines the decay length of the evanescent wave into the crystal, increases as one moves from gap edge to gap centre (figure 5). This aspect of the wavefunction will become important in part of our discussion in the next section.

Finally, we should comment on the fact that the phase accumulation model, and the graphical solutions of this as seen in figure 7, produce solutions which lie both inside and outside the energy limits of the substrate band gap; clearly, outside these limits the electrons are not truly in a confined well. Nevertheless, these states are observed to exist, and are the QW analogues of so-called surface resonances—effectively intrinsic Shockley-like surface states which do not fall in the substrate band gap. Because these states are outside the gap, they can couple to bulk states and are not truly localized at the surface. However, the wavefunction amplitudes of these surface and QW resonances are enhanced at the surface, and thus they do lead to enhanced photoemission intensity and share many of the characteristics of truly localized surface and QW states.

3. The role of periodic crystalline potentials in photoemission

In the treatment so far we have treated the metallic thin films as simple flat-bottomed wells with a thickness defined by the number of associated atomic layers. We know, of course, that in a bulk crystal, the periodic potential of the atoms within it leads to many of the established electronic properties of crystalline solids, such as the presence of pseudo-continuum bands and of band gaps at the Brillouin zone boundaries. This periodicity, and notably the fact that electron momentum can be changed in units of reciprocal lattice vectors by scattering off the crystal lattice, also has important consequences for angle-resolved photoemission experiments from valence states in solids. It is therefore helpful to summarize a few important results for extended solids (e.g. [51, 52]) as a reference for our discussion of the behaviour of thin films.

Probably the most significant such result is that optical transitions (those involving absorption or emission of a photon, as in photoemission) are ‘direct’ or ‘vertical’ transitions, involving no change in the reduced electron momentum in the solid. A free electron is unable to absorb the energy of a photon in a scattering experiment because the momentum carried by a photon is extremely small compared to that of an electron of similar energy, so energy and momentum cannot be simultaneously conserved. For an itinerant (perhaps nearly-free) valence electron in a solid, however, such a photon absorption can occur, because the crystal lattice can provide the necessary momentum recoil in the form of a reciprocal lattice vector. In the reduced-zone scheme of presenting a band structure the role of all possible reciprocal lattice vectors is automatically included, so photoemission involves a ‘vertical’ transition from an occupied state to an unoccupied state having (almost) the same reduced electron momentum. The consequences of this are illustrated in figure 12 for the case of Ag along the (100) bulk direction (the Γ–X direction in reciprocal space), specifically for photoemission from the occupied part of the nearly-free-electron-like s–p band, into unoccupied final states of the same symmetry. Clearly different photon energies sample different parts of the band structure, but by taking angle-resolved photoemission spectra along the surface normal of a (100) surface (and thus in the same direction as this part of the band structure) one sees the initial-state band dispersing in electron wavevector.

This strong selectivity in conserving the perpendicular component of the electron wavevector is actually slightly surprising; angle-resolved photoemission typically involves emitted electrons with kinetic energies in the range 15–150 eV, and at these energies the mean free path for inelastic scattering is very short. Certainly for electrons in the kinetic energy range of around

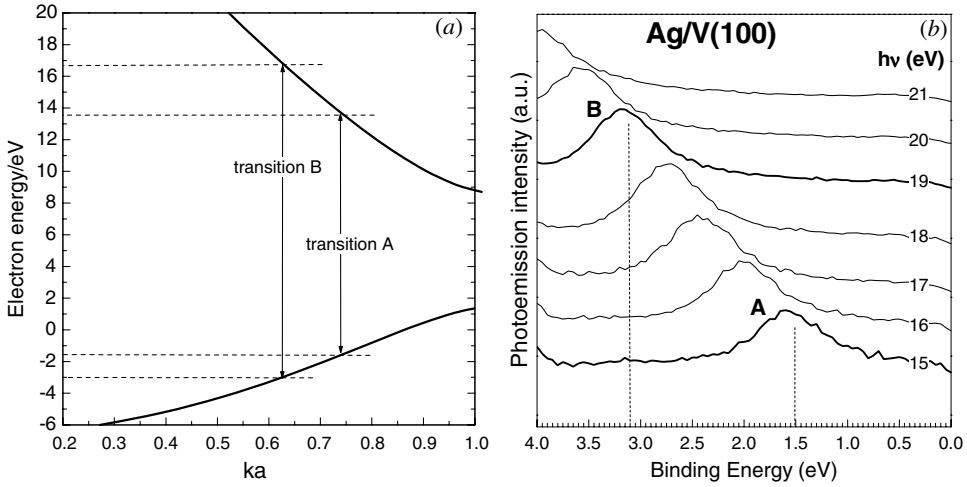

Figure 12. (*a*) Simple schematic of part of the s–p band structure of Ag showing direct transitions at different photon energies. (*b*) Presents a set of normal emission photoelectron energy spectra from a thick film of Ag grown on V(100) at different photon energies, showing the dispersion of the peak due to the direct transitions predicted by this simple diagram.

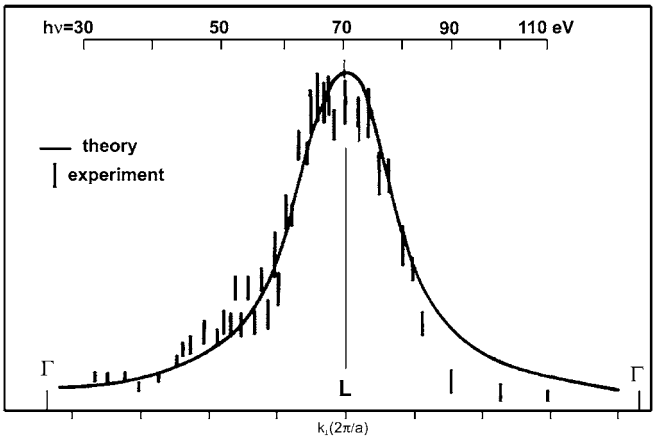

Figure 13. Intensity of the photoemission signal from the intrinsic Shockley surface state on Cu(111) as a function of photon energy in normal emission. The lower axis shows the electron momentum of the final-state photoelectron in terms of the bulk Brillouin zone (adapted from [53]).

40–150 eV this mean free path is only about 5–10 Å, although it can be significantly larger at 15 eV. In all these experiments the signal therefore arises mainly from the near-surface region. For a surface only the two-dimensional periodicity parallel to the surface is strictly retained, so while the parallel component of the electron wavevector, $k_{\parallel}$, should certainly be conserved, one would expect the perpendicular component, $k_{\perp}$, to be far less well defined. There must be some effective smearing of the final-state bands which are sampled in photoemission due to this limited sampling depth. However, data such as those of figure 11 clearly show that the measurements probe sufficient depth, and that the surface layers are sufficiently similar structurally and electronically to those of the bulk, that $k_{\perp}$ conservation is generally applicable (albeit with some smearing), despite the fact that 80% of the signal originates from only about 5–10 layers.

The situation is potentially quite different, however, if we consider angle-resolved photoemission from a very thin film. One might expect that, if the occupied electronic states are sufficiently localized in space (perpendicular to the surface), then the initial value of $k_\perp$ is ill-defined and the direct transition consideration is irrelevant. We should remark in this context that, unlike a free electron, an electron bound in a spatially localized state *can* be photoemitted with no problem of momentum conservation. For example, photoemission is routinely observed from bound states on free atoms; in this case the necessary momentum recoil is supplied by the far more massive nucleus, which can provide any arbitrary amount of momentum (the associated energy loss being trivial). A similar argument would apply to a hypothetical isolated ordered layer of atoms in free space; the ordering within the layer means that, for photoemission of an itinerant valence electron within the layer, the component of the electron momentum parallel to the layer, $k_\parallel$, will be conserved by a discrete recoil of a reciprocal net vector. However, perpendicular to the layer the electron is localized and the atomic layer can provide any arbitrary amount of recoil momentum, like the free atom. Of course, the situation we are interested in is not an isolated layer (or layers) of atoms in free space, but such an assembly of atoms on a crystalline surface. In this regard it is helpful to compare the situation with that of the far more completely characterized case of surface states at clean solid surfaces. As we have already indicated, these are electronic states which exist only at the surface within a projected bulk band gap of the substrate, and have associated wavefunctions which decay into the substrate. If these states are truly localized perpendicular to the surface, the situation is similar to that of the states in an atomic layer in free space; their associated value of $k_\perp$ becomes undefined, and one can plot such a state on a band structure like that shown in figure 12 as a line of fixed energy but of all possible $k_\perp$ values. If there is a dispersing unoccupied final-state band at higher energy, one can then draw a series of vertical lines (at constant $k_\perp$) and would predict that the state should be visible in photoemission spectra at any appropriate photon energy, with none of the dispersion seen in the spectra of figure 12.

However, experiment shows that, while such states do, indeed, show no dispersion in their binding energy with changing photon energy, the *intensity* of their associated photoemission peak is strongly dependent on photon energy. Indeed, the intensity is found to peak at photon energies which would correspond to $k_\perp$ conservation for a state with an initial $k_\perp$ value equal to that associated with the gap which the state occupies [53–55]. Figure 13 shows an early example of this for the surface state on Cu(111) [53] in the form of a plot of the dependence of the intensity of photoemission at normal emission as a function of photon energy from the Shockley surface state just below the Fermi level. The photon energies are shown along the top of the graph while at the bottom the final-state energies are converted into $k_\perp$. The bars are the experimental points while the full curve is the result of a theoretical simulation based on direct transitions to bulk final states of the solid. The generally accepted explanation of this effect is that the oscillatory evanescent tail of the wavefunction has the periodicity of this initial $k_\perp$ value, and it is this dominant Fourier component that effectively imposes a strong remnant of $k_\perp$ conservation, even for this surface-localized state. Notice, however, that these surface states can be described within the phase-accumulation model, as described in the previous section, and the solution of this model defines a value of k (perpendicular to the surface) for the electron wave trapped by the image potential and the crystal barrier. Moreover, as the energy of the surface state falls within the substrate gap, the associated k value is inevitably close to that for the gap state within the substrate. The experimental observation of the optimum energies for observation of the surface state in photoemission is also compatible with this value of k, establishing the conditions for the direct transition.

If we now turn to QW states associated with thin epitaxial films, it is immediately clear that one key question we might ask is whether the periodicity of the substrate and/or the atomic

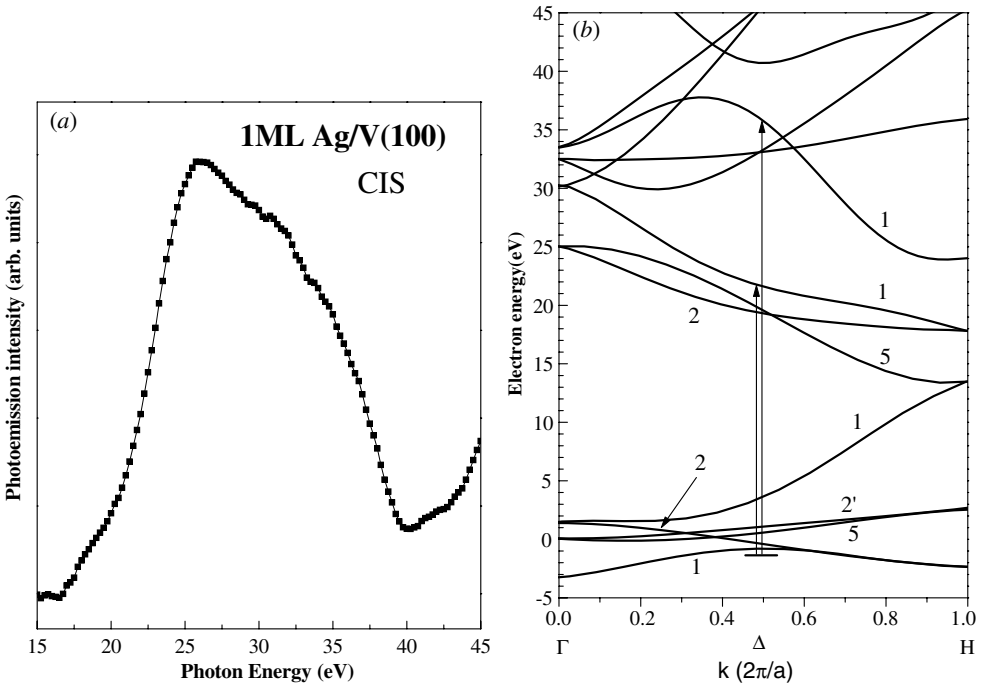

Figure 14. (*a*) Photon energy dependence of the photoemission intensity (CIS spectrum) from the QW state in a 1 ML Ag film on V(100). (*b*) V band structure in a direction perpendicular to the (100) surface. Possible direct transitions from the 1 ML Ag QW state into s–p final-state bands of the substrate of Δ_1 symmetry are indicated by arrows [56].

layers within the film imposes a strong photon energy dependence of the photoemission cross section through similar $k_\perp$ conservation. For a single atomic layer film, it is clear that, if such an effect occurs, it can only be via a direct transition into a final state defined by the band structure of the substrate. Indeed, one such example is that of a QW state associated with a single monolayer (1 ML) of Ag on V(100), and the photon energy dependence of the photoemission cross section in this case is consistent with direct transitions to V(100) substrate final states, a very direct analogue of the situation of intrinsic surface states of clean surfaces [56]. Figure 14(*a*) shows the intensity of the photoemission from this QW state as a function of photon energy (a so-called constant initial state—CIS spectrum). A broad peak is seen which clearly comprises at least two separate features at photon energies of approximately 25 and 35 eV, and as is shown in the band structure of figure 14(*b*) these correspond well with the expectations for direct transitions from the QW state (superimposed as a short bar at the appropriate energy and k value) into the symmetrically compatible Δ_1 final-state bands. By contrast, if the film is thick enough, its behaviour should be essentially identical to that of a bulk crystal of the overlayer film material (albeit perhaps in a structural phase which is imposed by the epitaxial growth). The thickness at which these direct transitions to bulk-like final states of the film band structure become important is a matter of some debate. A rather clear illustration of the expected pattern of behaviour is provided by the results of some calculations for isolated films, comprising a small number of layers modelled in a very simple fashion by one-dimensional chains of atoms, by Henk and Johansson [57]. These calculations indicate that, even for a five-layer film, peaks are expected in the intensity of the QW photoemission

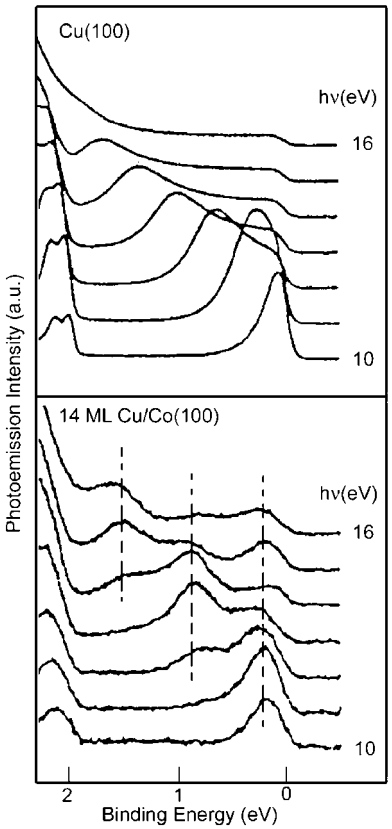

Figure 15. The upper panel shows a set of normal emission photoelectron energy spectra from a Cu(100) surface recorded at different photon energies. The lower panel shows a similar set of spectra from the 14 ML film of Cu on fcc Co(100); the broken lines show the energies of three coexisting QW states in this film (adapted from [58]).

at photon energies corresponding to direct transitions to the final states compatible with an infinitely thick overlayer. However, the width of this peak in intensity versus photon energy is larger for thin films (short chains) than for thicker films (longer chains) due to a kind of k smearing resulting from the small number of layers.

Experimental evidence for this kind of direct transition of QW state photoemission to bulk final-state bands of the overlayer material has been published for the case of Cu films on fcc Co(100). Figure 15 shows data [58] from a 14 ML film which certainly suggests that this number of layers is sufficient to permit direct transitions from QW states to bulk final-state bands of the overlayer film. The upper panel of figure 15 shows a set of normal emission photoelectron energy spectra from a Cu(100) surface recorded at different photon energies, and shows how the photoemission peak follows the dispersing Cu s–p band due to the importance of direct transitions, exactly like that seen for Ag(100) in figure 12. In the lower panel is shown a similar set of spectra from the 14 ML film of Cu on Co(100); the broken lines show the energies of three coexisting QW states in this film, and the photoemission intensity switches between them in a fashion entirely consistent with direct transitions to the same Cu(100) final states. More recently, data have been presented for this same fcc Co(100)/Cu system which appear to support the view that this kind of direct transition may occur for films as thin as 3 ML, apparently

with little evidence of smearing of the k conservation due to the very thin film [59]. In this regard more complete calculations of the Co(100)/Cu system (which take explicit account of the substrate) by Henk and Johansson [57] are relevant, because, although they show a trend for this kind of direct transition to remain important even for rather thin films, they also show that other processes can become important for such very thin films. Indeed, as we will discuss in the next section, experiments on other systems show quite different behaviour, and provide evidence for fundamentally different mechanisms influencing the photoemission yield as a function of photon energy. We will therefore defer further discussion of this aspect of the role of the periodic atomic potential in QW photoemission until the next section.

A more general consequence of the presence of a periodic atomic potential in the overlayer film, however, is that we have the possibility of Bragg scattering, leading to the idea that Bloch functions should be used as the proper way to describe propagating electrons in the initial QW state, as well as the final photoelectron state. Strictly, of course, Bloch's theorem only applies to an infinite (ideally periodic) system, but some vestige of this effect might be expected to appear even for films of only a few atomic layers. An important consequence of this is that, within the phase accumulation model, the electron wavefunctions should no longer be described as a sum of two waves, travelling in opposite directions (with wavevectors k and $-k$) and resulting from reflections at the film boundaries, but instead by *four* waves, the two already considered and two additional components which correspond to the Bragg reflections of each of these. These two additional waves have wavevectors $(k–g)$ and $-(k–g)$, where g is a reciprocal lattice vector. Commonly, QW states occur with k values which are reasonably close to a Brillouin zone boundary. This is because such states must occur in a substrate band gap (and hence must have real components of k in the substrate which are at such a boundary), and if the overlayer film layer spacing is similar to that of the substrate this will often mean one is also reasonably close to a band edge in the film. For different structural phases, of course, this need not be the case. If it is so, however, then the QW wavevector k and its Bragg-scattered wavevector $(k–g)$ will be closely similar, and combining them will produce a modulating envelope (similar to the effect of beats in classical waves) with a spatial period much longer than that of the original electron wave. The consequence of combining all four waves is thus to produce a spatially modulated standing wave. This modulation is commonly referred to as the *envelope function*, and some recent discussion of QW states has implied that this modulation is actually the dominant property of the associated wavefunctions (e.g. [59] although this is not really correct [4]). Part of this confusion arises from writing the phase accumulation condition in a different way. Earlier we argued that the key condition for a standing wave is

$$\phi_B + \phi_C + 2kd = 2\pi n. \tag{8}$$

Notice, however, that $d = Na$ and the reciprocal lattice vector perpendicular to the surface associated with the first Brillouin zone is $g = 2k_{BZ} = 2\pi/a$ so $2k_{BZ}d = 2N\pi$, which means that one can rewrite equation (4) as

$$\phi_B + \phi_C + 2(k - k_{BZ})\, d = 2\pi(n - N)$$

or

$$2(k_{BZ} - k)\, d - (\phi_B + \phi_C) = 2\pi v. \tag{9}$$

Now $(k_{BZ}-k)$ is the wavevector of the envelope function, so equation (9) appears to show that it is the matching of the envelope function phase which is the fundamental requirement. In truth, however, we have simply added the same amount of phase to both sides of equation (8), and the result is really more an issue of 'book-keeping' than of fundamental physics. Equation (9) would be no less true if there were no significant periodic atomic potential in the film and thus no significant Bragg scattering (and hence no envelope function). Furthermore, the energy of

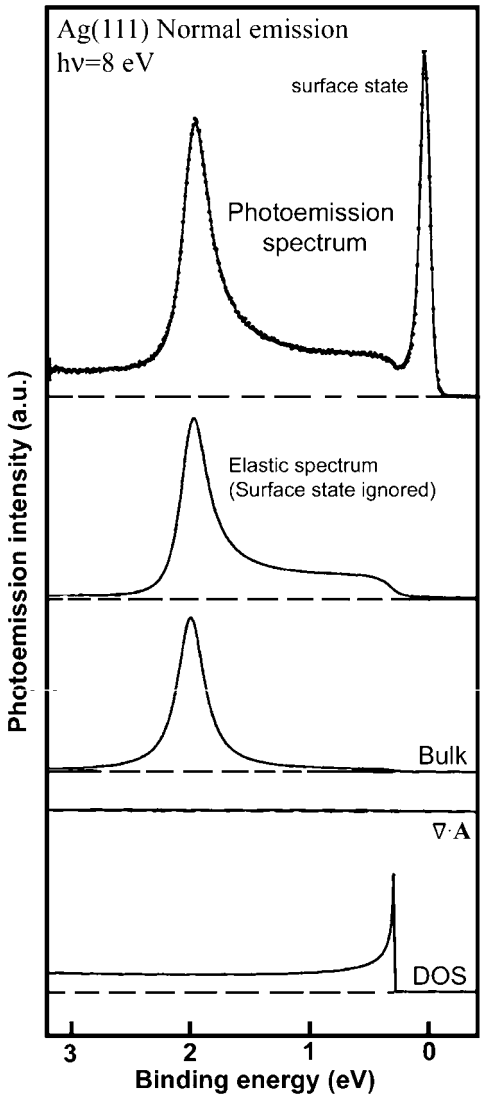

Figure 16. From top to bottom: the experimental spectrum (dots) and a model fit (full curve) of the Ag(111) photoemission spectrum in normal emission at a photon energy of 8 eV; theoretically predicted elastic photoemission spectrum from this surface ignoring the surface state; the same model spectrum calculated by retaining only the bulk component; elastic spectrum calculated by retaining only the $\nabla \cdot \boldsymbol{A}$ component; and the DOS of the initial states probed in this experiment (adapted from [60]).

the QW state is determined by k, and this value is found from matching the associated electron wavelength to the well as defined by equation (8), with no reference to the Brillouin zone wavevector. What equation (9) shows, however, is that, having achieved this matching in k, one also has a similar matching of the envelope arising from the Bragg scattering within the periodic potential of the film.

A key question, of course, is 'what are the observable consequences of the envelope function?' In truth, the answer appears to be very few. One rather elegant experiment [60]

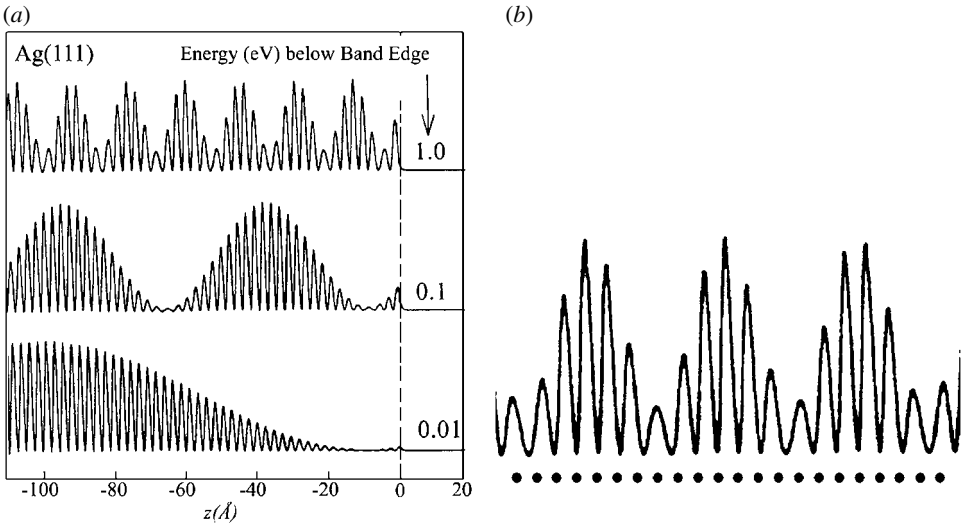

Figure 17. Sketches of the charge distribution of the s–p band states near the surface of Ag(111) (at $z = 0$) at different binding energies relative to the top of the band edge, obtained by regarding the sample as a very thick film still bounded by the outer surfaces and thus treatable as a quasi-continuous set of QW states. Note the envelope-function modulations. The right hand panel shows a section of the upper charge distribution of the left-hand panel, with dots superimposed to show the positions of the atomic layers (adapted from [60]).

which does demonstrate the potential importance of the envelope function actually arises from a study of the photoemission from an Ag(111) surface with no overlayer film; nevertheless, the presence of the free surface(s) of this bulk crystal means that it behaves like a very thick film which must still have an envelope function matched at the surfaces. At the top of figure 16 is shown the photoelectron energy spectrum obtained at normal emission from this surface. It comprises three main features. At a binding energy of approximately 2 eV is a peak arising from a direct transition from the bulk s–p band of Ag, while the narrow peak just below the Fermi level is due to photoemission from an intrinsic (Shockley) surface state on the surface. Between these two is a low plateau of emission with a rounded edge a few tenths of an eV below the Fermi level. This is attributed to indirect transitions from the s–p band of the bulk; the upper edge of this band then corresponds to the step in the spectrum just below the energy of the surface state (which lies, of course, within the band gap above this band edge). The origin of this s–p band indirect transition background is actually so-called surface photoemission. The matrix element for photoemission from an initial state ψ_i into a final state ψ_f comprises two terms:

$$\langle \psi_f | 2\boldsymbol{A} \cdot \nabla + \nabla \cdot \boldsymbol{A} | \psi_i \rangle = M_b + M_s \tag{10}$$

the first term being the normal ('bulk') photoemission and the second the surface photoemission. The surface photoemission arises from the change in the vector potential $\boldsymbol{A}$ which occurs as one passes from the vacuum into the solid; this term is commonly ignored in photoemission, and in the case of a continuous medium this term is zero. It is the interference of the bulk and surface terms which is used to explain the details of the shape of the bulk peak and the broad background in the spectrum of figure 16; notice that the bulk term alone gives a symmetrical peak for the s–p band direct transition. Of especial interest in the present context, however, is the s–p band *indirect* transition contribution to the spectrum. One would expect

this to reflect the density of states (DOS) of this bulk band, but as is shown in the bottom of figure 16, this should show a singularity at the top edge of the band as the band dispersion falls to zero at the bottom of the gap. Clearly, the predicted and measured surface photoemission contributions do not show this sharp peak in the DOS. The reason for this is the changing form of the envelope function in the vicinity of the surface as one approaches the band edge, as shown in figure 17. The surface boundary matching condition in this system is such that a node occurs very close to the surface. As the energy increases, and the associated k approaches the band edge and a value of k_{BZ}, the wavelength of the envelope function becomes very long, causing the associated wavefunction to have a very small value in the near-surface region (within the inelastic scattering mean free path). Thus, in the energy range of the DOS singularity, the wavefunction amplitude is so small that there is no photoemission contribution, and the band edge appears rounded off in the spectrum.

Notice, incidentally, that the sketches of $|\psi|^2$ shown in figure 17 show the situation as one approaches the top of a band and the wavevector k approaches k_{BZ}; the wavevector determining the periodicity of the envelope function, $(k_{BZ} - k)$, then becomes very small and the wavelength becomes very long. The opposite situation occurs, of course, near the zone centre when k is very small, $(k_{BZ} - k)$ is large, and the 'envelope' function actually produces a short-wavelength weak modulation of the wavevector k [46]. This is the situation in the laterally confined surface state seen in the STM results of figure 3; this surface state is at the zone centre at the lowest energy, and even at the highest energies shown in this figure it is far from the zone edge. These STM images thus show no visible influence of any envelope function.

A photoemission study aimed more directly at probing the envelope function in thin film QW states is the Cu/Co wedge experiment [49] which has already been mentioned earlier. In the previous section we showed in figure 8 the results of a photoemission study from a wedge-shaped film of Cu grown epitaxially on fcc Co(100). This experiment actually involved the deposition of *two* Cu wedge films, with their directions of increasing film thickness at right angles to one another, these two wedges being separated by a 1 ML film of Ni. This sample structure is shown schematically in the upper part of figure 18; notice that, in moving from corner B to D the overall film thickness remains constant, but the position of the Ni spacer layer shifts from the top to the bottom of the film. By contrast, traversing from A to C one has a linearly increasing film thickness, but with the Ni spacer layer always at the midpoint of the film thickness. The data shown in figure 8 were obtained by traversing from A to C with *no* Ni spacer layer. The lower panel of figure 18 shows how the photoemission intensity at the Fermi level changes as one scans over all lateral positions on the double wedge. There are clearly modulations in intensity as one moves parallel to the direction AC which are consistent with picking up photoemission from states of different ν values at the Fermi level as one increases the film thickness. These are essentially the same modulations seen in figure 8 for varying film thickness at the Fermi level (i.e. moving along the top edge of the data panel of figure 8).

Also seen in the data of figure 18, however, are modulations as one traverses the film parallel to BD, for which the total film thickness is unchanged but the position of the Ni spacer changes. The Ni film should act as a weak scattering barrier to the Cu QW states at energies close to the Fermi level, so the data have been interpreted in terms of the effect of this barrier in identifying the locations of the nodes and antinodes of the QW envelope function. The situation is somewhat analogous to that of lightly touching a vibrating string; if one touches the string at the position of a node in its vibration, there is little effect, but if one touches the string at the position of an antinode one strongly damps the vibration. Moving the Ni spacer layer through the film is thus analogous to moving the touching finger along the string, so the spatial periodicity of the modulations in the photoemission intensity along BD are a measure of the wavelength of the envelope function. Strictly, the situation here is exactly the

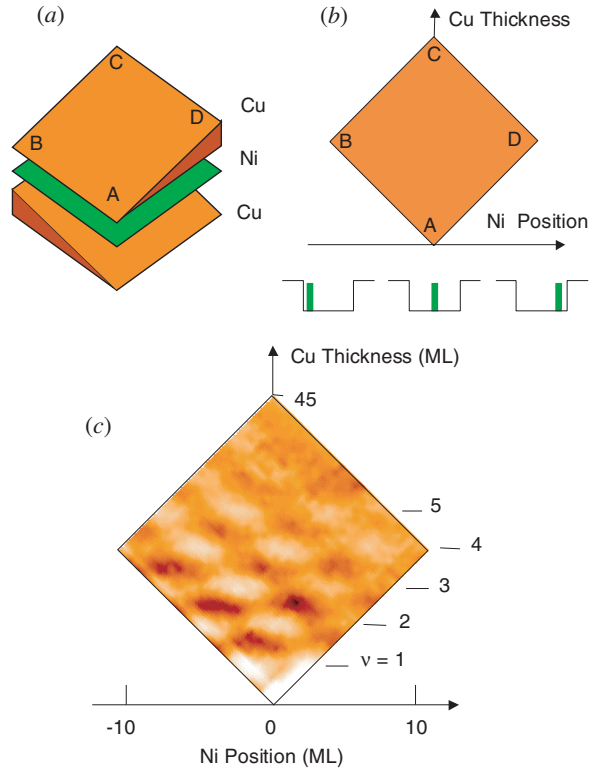

Figure 18. Experimental geometry and results of a photoemission experiment to study QW states in a novel Cu wedge film grown epitaxially on fcc Co(111). (*a*) and (*b*) show the sample schematically. The exploded view (*a*) shows the two Cu wedge films, mutually rotated by 90°, and separated by a 1 ML nickel film. A plan view is shown in (*b*) above a schematic of the resulting electron potential perpendicular to the film surface at three positions along the line BD (for which the total Cu film thickness is constant). (*c*) Shows a half-tone map of the photoemission intensity from states at the Fermi level as a function of position on the sample surface (from [49]).

opposite to the touching string analogy, because the scattering phase shifts in this system are such as to place antinodes close to the boundaries, with the consequence that the QW state is damped when the Ni spacer is positioned at a node rather than an antinode. Notice too that an important aspect of this elegant experiment is that the Ni film does not totally decouple the QW state wavefunctions in the Cu films on either side of the spacer layer for states near the Fermi level; in fact, this decoupling *does* occur at lower electron energies for which the Ni presents a stronger barrier [49].

We should, perhaps, finally comment briefly on the physical significance of the envelope function. As is well known, the wavefunctions associated with s–p character bulk electronic states at the bottom and top of a band gap both have wavelengths of twice the lattice parameter (i.e. have $k = k_{BZ}$) but the state at the bottom of the gap places the charge accumulation between the atoms (p-like bonding character) and is thus of lower energy than the alternative phase represented by the state at the top of the gap which places the charge accumulation *on* the atoms (s-like anti-bonding character). For these states exactly at the gap the envelope function has zero wavevector (infinite period)—i.e. there is no modulation. As we move away from the gap, k is no longer commensurate with the lattice, so whatever the phase relationship of

the QW standing wave to the atomic positions, there must be positions where the local charge accumulation is locally on the atoms, and others where it is between the atoms. Placing charge at the atomic positions costs energy, and what the envelope function does is to suppress the amplitude at these positions, whereas the maxima in the envelope function correspond to the positions where the charge accumulation is between the atoms (see the right-hand sketch of figure 17). This modulation thus results in a lowering of the energy relative to that which would occur if there was no such amplitude modulation.

4. Photon energy dependence of quantum well photoemission

In the previous section we have already discussed the way in which direct transitions from QW states, having a well-defined energy and $k_\perp$, to final states of the substrate or overlayer film band structure may influence the intensity of the photoemission signal. There is clear evidence from some QW systems, however, that other effects can be even more important. One such effect has been attributed to an interference between photoemission arising at the substrate/film and film/vacuum interface. The origin of this physical description arises from a very simple model of the QW potential and the associated use of one specific form of the photoemission matrix element. We have already given the general form of this matrix element in equation (10), and if we make the usual assumption that the $\nabla \cdot \boldsymbol{A}$ term is zero, we are left with a matrix element of the form

$$\langle \psi_f | \boldsymbol{A} \cdot \nabla | \psi_i \rangle. \tag{11}$$

If we neglect the spatial variation of the vector potential (make the so-called dipole approximation) then the core of the matrix element becomes simply $\langle \psi_f | \nabla | \psi_i \rangle$. This is sometimes referred to as the dipole-velocity form of the matrix element, but one can show that two alternative forms are equivalent which are (but for some constants) $\langle \psi_f | \boldsymbol{r} | \psi_i \rangle$, the dipole-length form, and $\langle \psi_f | \nabla V | \psi_i \rangle$, the dipole-acceleration form (where V is the potential). In one dimension these three forms become $\langle \psi_f | \partial/\partial z | \psi_i \rangle$, $\langle \psi_f | z | \psi_i \rangle$ and $\langle \psi_f | \partial V/\partial z | \psi_i \rangle$. Reverting now to the simple rectangular well description of the QW, the dipole-acceleration form involves taking the derivative of this potential, which leads to delta functions at the two boundaries. The matrix element thus has two terms which involve the amplitudes of the initial- and final-state wavefunctions at the two boundaries; the modulus squared of this matrix element, which is proportional to the photoemission flux, will therefore involve interference between these two terms. As the final-state wavefunction and wavevector depend on the photon energy, we can thus expect to see modulation in the interference of these two spatially separated sources. Of course, this description is based on a highly simplified picture of the true potential, yet it identifies a wholly different physical process which may be explored.

The first evidence for this type of effect was found in photoemission studies of thin films of Na and Cs on Cu(111) but only at very low photon energies (up to 8 eV for 4–7 ML films and up to 25 eV for 1 ML films) [61,62]. Although these experiments did show an oscillatory dependence of the intensity on photon energy, the data range was only long enough to show a single oscillation. We therefore concentrate here on our own data for the V(100)/Ag system which covers a wider range of photon energies and film thicknesses [47]. A set of photoelectron energy spectra from these QW states has already been shown in figure 6. Figure 19(*a*) shows the measured photoemission intensity from these six different QW states as a function of photon energy (constant initial-state spectra) in the range 15–45 eV, while figure 19(*b*) shows the results of a simulation of these data based on a very simple asymmetric rectangular well model which takes no account of the nature of the substrate and the associated phase shifts, nor of the corrugation potential within the well and the image potential at the film/vacuum

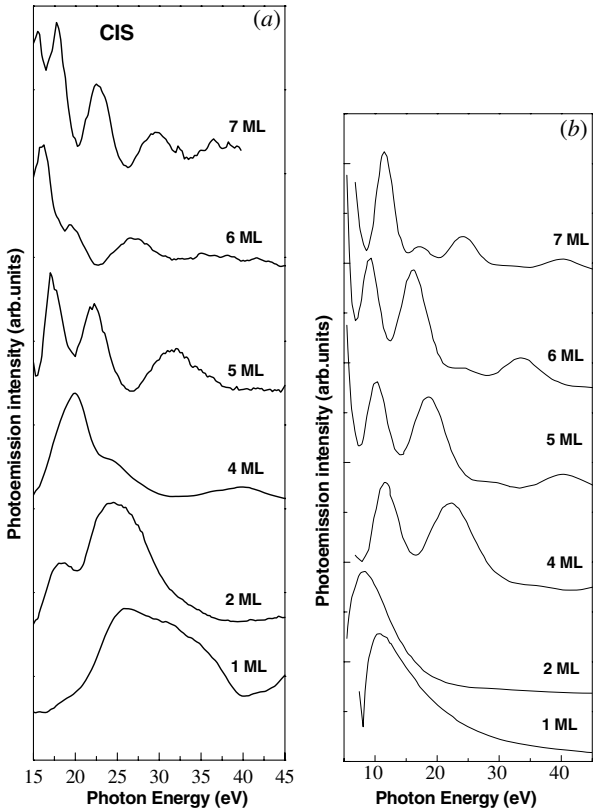

Figure 19. (*a*) CIS spectra showing the photon energy dependence of the photoemission intensity from QW states in several different thicknesses of Ag films on V(100). (*b*) Theoretical simulations of the CIS spectra shown in (*a*) from [47].

interface. While the quantitative agreement between these experimental and theoretical results is poor, the theory clearly reproduces much of the systematic behaviour of the experimental results. In particular, both theory and experiment show strong oscillations in the photoemission cross section and in both the number of oscillations increases as the film thickness increases. By contrast, of course, because the energy and $k_\perp$ values of all the QW states are quite similar (they must all fall in the 0 to -2 eV range of the band gap below the Fermi level), any direct transition should lead to a very similar photon energy dependence for all of these states. In fact, the broad peak for the 1 ML state, which could evidently be separated into two or more components, *can* be reconciled with direct transitions to final states of the bulk V(100) substrate (as discussed earlier by reference to figure 14), but there are *no* appropriate final states for bulk Ag to which direct transitions could occur in this photon energy range.

This situation contrasts rather strongly with the conclusions of an investigation of the fcc Co(100)/Cu system mentioned in the previous section [59] in which photoemission from QW states associated with 3 and 6 ML films were found to show strong enhancement at the photon energies of approximately 14, 82 and 120 eV, all consistent with direct transitions to bulk Cu final states. The origin of this very different behaviour is currently unexplained. As a very general statement, one can argue that both direct transitions and surface/interface interference effects should be possible, but the question remains of why one process seems to dominate in

the case of V(100)/Ag and the other in the case of fcc Co(100)/Cu. It is also quite surprising that, even for a Cu film as thin as 3 ML, a direct transition to a bulk Cu final state is implicated. There are two key differences between these different combinations of substrate and overlayer which may be important in understanding this result.

The first concerns the nature and quality of the overlayer films. In the case of V(100)/Ag the Ag films appear to be extremely uniform, at least for films up to a few ML thickness [63,64]. This is manifest in the fact that the photoemission spectra show sharp clearly resolved single QW peaks associated with unique films comprising an integral number of layers; films of intermediate average thickness comprise films of two different thicknesses with two distinct QW peaks which are well separated and provide a spectroscopic signature of an inhomogeneous film (e.g. figure 9). By contrast, all the published results on the fcc Co(100)/Cu, system, which has been studied extensively by several groups [49,65–70], seem to indicate relatively rough and inhomogeneous films. We have already remarked on this in relation to the apparent *continuous* evolution of QW state energies with film thickness in figure 8. The more recent study of the photon energy dependence, apparently dominated by the effect of direct transitions, shows spectra in which several different layer thickness contributions are evident in all the spectra, and while it may be possible to separate these in the higher resolution spectra at low photon energies, this is unlikely to be true at the higher photon energies. As remarked above, the direct transition photon energies are very similar for the different QW states, so even if one averages over several different states the photon energy dependence will be similar. By contrast, the surface/interface interference phenomena are quite different for different QW states, so averaging over several states would wash out much of the interference effect, leaving, perhaps, an underlying effect due to direct transitions. For very thin films, however, the energy of the QW states can change significantly for thickness differences of one layer, and the possible roughness is constrained by the small average thickness, so it seems unlikely that this effect is sufficient to explain the pronounced differences observed.

Apart from this issue of the quality of the films in these different systems (which appears to be an intrinsic property rather than any reflection on the care taken by the experimenters), there is a fundamental difference in the nature of the bulk final states available in the two substrate/film combinations. In the case of V(100)/Ag, the V substrate is bcc, whereas bulk Ag is fcc, and even in the pseudomorphic growth of Ag on V(100), the structure of the Ag film will only be modestly strained from this bulk phase. As a consequence k_{BZ} along the [100] direction is quite different in the substrate and the overlayer, so the higher bands (folded in from higher Brillouin zones) also differ strongly. By contrast, the Co substrate used in the Co(100)/Cu studies is the fcc phase, which is actually grown as a thin film pseudomorphically on a Cu(100) substrate, so both substrate and overlayer are fcc with almost identical lattice parameters. Co and Cu are also very close in the periodic table and thus are very similar electron scatterers, so the higher-energy final-state s–p bands should be very similar. In this case we can envisage strong coupling between substrate and overlayer states. This may explain why only 3 ML of Cu behaves as though it already has a well-defined bulk band structure; the actual final states may really be slightly modified extensions of the wavefunctions of the underlying Co substrate bands. Indeed, if this argument is correct, it means that the clear evidence for direct transitions from QW states in a 14 ML Cu film on fcc Co(100) seen in figure 13 may not indicate that even 14 ML is *generally* sufficient to fully form bulk-like final-state bands for QW state photoemission. This same type of coupling is not possible in the V(100)/Ag case. Clearly it would be interesting to explore this idea further, by trying to establish the systematics of other substrate/film combinations. One system which has been studied quite extensively and which might be expected to behave like V(100)/Ag is Fe(100)/Ag (e.g. [37,41,46,71] and references therein). Some data on the photon energy dependence of QW photoemission from

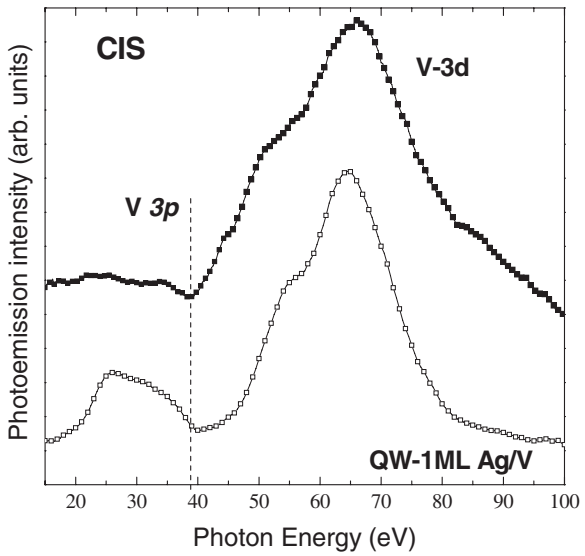

Figure 20. CIS spectra showing the photon energy dependence of the photoemission intensity from the clean V(100) 3d band and from the QW state in a 1 ML Ag film on V(100). The vertical line indicates the V3p threshold energy (adapted from [74]).

this system have been published, but only over very narrow photon energy ranges [72], so it is difficult to evaluate the results in the context of these two distinct mechanisms.

Finally, we should mention one rather special source of photon energy dependence in photoemission which appears to play an important role in the case of the QW state in a 1 ML film of Ag on V(100), namely interatomic resonant photoemission. The phenomenon of resonant photoemission is now well established and has been observed in many materials [73]. In vanadium, for example, when the incident photon energy matches the threshold for photoexcitation of the 3p state to the unoccupied part of the 3d band, coherent interference can occur between the direct photoemission from the valence band and the autoionization involving this transition. In the simplest cases the effect leads to a characteristic Fano lineshape in the photon energy dependence of the photoemission cross section at the resonance. Figure 20 shows the results of measurements of the photoemission intensity from the QW state of the V(100)/1 ML Ag system, and from the V 3d state on a clean V(100) surface, as a function of photon energy from 15–100 eV [74]. The lower energy part of this constant initial-state spectrum from the QW state, up to 45 eV, has already been presented in figure 14 and discussed in the context of direct transitions to V bulk final-state bands. In the photon energy range from around 50 to 80 eV, however, there is a very strong enhancement of the photoemission cross section, which is essentially identical in shape and magnitude to that of seen in the V 3d photoemission from the clean substrate. This 3d emission enhancement is characteristic of the resonant photoemission of valence band photoemission in V, which is well known to produce a broad peak in the photon energy range around 65 eV which appears above the V $3p \rightarrow 3d$ transition at approximately 37 eV [75]. The clear similarity of this feature in the two CIS spectra of figure 20 indicates the existence of an interatomic resonance in which the QW state must participate in the decay of the V $3p \rightarrow 3d$ excitation. The decay of the excited state ($[3p^5 3d^{n+1}]^* \rightarrow 3p^6 3d^{n-1} + e$) is, of course, essentially equivalent to an Auger process except that in the normal Auger process the initial core excitation is into the continuum and the final state is a two-hole, rather than a one-hole, state. Nevertheless, the requirements for interatomic resonant photoemission should be somewhat similar to those for interatomic Auger

processes which have been known to occur for many years in conventional Auger electron spectroscopy [76]. In general, however, interatomic Auger effects have been associated with the rather ionically bonded systems in which the valence charge is largely localized on the anion, so if a shallow core hole is created on the metal cation the only decay mechanism is via the anion valence electrons. Interatomic Auger processes also form the dominant route for neutralization in low energy He^+ ion scattering from metals, the He^+ ion again having no shallower valence electrons to permit an intra-atomic Auger process (e.g. [77]).

Clearly this situation does not pertain in the case of a metallic overlayer on a metallic substrate. However, we can anticipate that the QW state wavefunction for the 1 ML Ag overlayer will have significant overlap with the outermost V layer atoms, so one can certainly imagine that coupling to the V autoionization process is possible. In this context we note that, in the V(100)/Ag QW system, the effect is only seen in photoemission from the 1 ML QW, and not in emission from QW states of thicker films, when the QW state will have a much reduced overlap with the substrate V atoms. In the past, because resonant photoemission requires significant coupling of the valence photoemission to the localized core state, resonant photoemission has been used in studies of valence band photoemission lineshapes in compounds and alloys (e.g. [78–80]) to associate different parts of the valence band with the constituent elements. If interatomic resonance is highly probably, as appears to be the case here, this previous underlying assumption may be unsound. So far, this is the only reported example of this interatomic resonant photoemission from a QW state; it is also, however, the only 1 ML system which appears to have been studied over an appropriately large photon energy range, so it is not really possible to know if the effect is essentially unique or quite common.

5. The temperature dependence of quantum well energy states

What happens to the photoemission spectra from the QW states as one changes the temperature? We might expect at least three effects: changes in the peak energy, changes in the peak intensity, and changes in the peak width. In this section we concentrate on the influence of temperature on the binding energies of the QW states, and defer a discussion of lineshapes to the following section. Experiments on the temperature dependence of the peak energy yield an apparently simple solution: because the film thickness suffers thermal expansion with increasing temperature, the associated wavelength increases and so the bound state energy decreases—i.e. the state becomes more strongly bound. In fact, this basic effect was observed, as reported in the introduction, in early electron reflectivity studies of thin films of Au on Ir(111) by Thomas in 1970 [5]. In these experiments, of course, the electron energies were a few eV above the vacuum level and probed unoccupied states. Recently, photoemission studies from occupied QW states in Ag films of V(100) have shown this same qualitative effect [81] and the main quantitative results are summarized in table 1. Figure 21(*a*) shows an example of some data from this investigation; the photoelectron energy spectra from a 2 ML Ag film are shown at different temperatures, and the peak associated with the QW state clearly shifts to higher binding energy as the temperature is raised. Figure 21(*b*) shows that this shift is linear in temperature, with a gradient of 1.6×10^{-4} eV K^{-1}. This superficially obvious result was actually not wholly expected. In all previous studies of the temperature dependence of bound valence state energies in solids the binding energies have been found to *decrease* with increasing temperature. This is also true for the energies of Shockley surface states, for example on Cu [82], Ag [83], Au [83] and Ga [84]. The origin of this effect is believed to be that the thermal expansion of the crystal leads to a lowering of the electron density and thus a reduction of the Fermi energy [85]. The problem is therefore one of the nature of the measurement. Clearly if we have a simple square potential well, thermal expansion increases the size of the well and lowers the energy of the bound states *relative to*

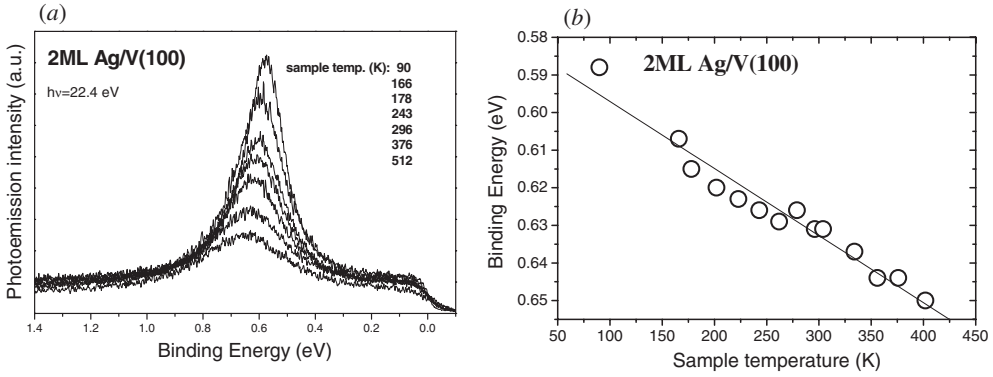

Figure 21. (*a*) Normal emission photoelectron energy spectra showing the peak from the QW state of a 2 ML Ag film on V(100), recorded at different sample temperatures. (*b*) Temperature dependence of the binding energy of the QW state taken from the spectra shown in (*a*) (adapted from [81]).

Table 1. Summary of the properties of the occupied QW states seen in Ag films on V(100) up to 8 ML thickness. The binding energy and number of nodal planes are as discussed in earlier characterizations of this system [47,87]. The right-hand columns show the results of a temperature-dependent study [81].

Film thickness (ML)	Binding energy (eV) at 90 K	No of nodal planes	Thermal shift (eV K^{-1}) ($\times 10^{-4}$)	Electron–phonon coupling, λ
0 (surface state)	At Fermi level	0	—	1.45 ± 0.15
1	1.65 ± 0.01	0	1.5	0.21 ± 0.05
2	0.58 ± 0.01	1	1.6	1.00 ± 0.03
3	No occupied state	—	—	—
4	1.43 ± 0.01	2	1.0	0.28 ± 0.12
5	0.82 ± 0.01	3	1.6	0.52 ± 0.07
6	0.36 ± 0.01	4	1.8	0.44 ± 0.07
7	1.44 ± 0.01	4	—	—
8	1.02 ± 0.01	5	1.1	0.25 ± 0.15

the bottom of the well. However, in a solid one measures the bound state energy relative to the Fermi level, and this energy, relative to the bottom of the well, also changes with temperature.

What is actually observed in a real experiment thus depends on the relative importance of these two conflicting contributions, and these may be deduced from the thermal expansion coefficients of the substrate and overlayer materials. In the case of the V(100)/Ag experiments the two relevant values for the constituent bulk materials are 17×10^{-6} K^{-1} for Ag and 8×10^{-6} K^{-1} for V, respectively. These values clearly favour the dominance of the increasing Ag film thickness over the expanding substrate. Of course, the bulk thermal expansion coefficient of Ag is not strictly appropriate to the pseudomorphic overlayer film which is centred tetragonal. Indeed, if we note that for a pseudomorphic Ag film on V(100) the thermal expansion of the film parallel to the surface is constrained to the low value dictated by bulk V, we can anticipate that the expansion coefficient in the Ag film perpendicular to the surface will be even larger than that in bulk Ag.

It is rather straightforward to quantify these arguments. In the case of a simple free-electron metal the Fermi energy, E_F, is proportional to the reciprocal of the square of the lattice parameter, so it is easy to show that the temperature dependence of the Fermi energy due to thermal expansion of the crystal is given by

$$dE_F/dT = -2E_F\alpha_S \tag{12}$$

where α_S is the coefficient of linear expansion of the solid substrate. Applying this model to the vanadium substrate, with a value for E_F of 5.2 eV, we obtain a temperature dependence of the Fermi energy of -8.3×10^{-5} eV K^{-1}. The fact that vanadium is a transition metal, rather than a free-electron metal, will have the effect of reducing the temperature dependence of the Fermi energy by a factor determined by the effective masses of the bands which cross the Fermi level. If the overlayer film thickness has a coefficient of thermal expansion of α_F, a QW state with an energy (relative to the bottom of the s–p band) of E_{QW} will have a temperature dependence of

$$dE_{QW}/dt = -2E_{QW}\alpha_F. \tag{13}$$

The QW state energy in the Ag film is measured from the bottom of the tetragonally centred silver overlayer s–p band whose dispersion perpendicular to the surface is determined experimentally to be -6.4 eV from the Fermi level [86], so for the 2 ML state with a binding energy relative to the Fermi level of 0.6 eV, we take E_{QW} as 5.8 eV. Equating the expansion coefficient of the film thickness to the linear coefficient of bulk silver then yields a result of -19.7×10^{-5} eV K^{-1}. This would predict an increase of the QW state binding energy relative to the Fermi level of 1.14×10^{-4} eV K^{-1}, somewhat smaller than the experimentally measured value for the 2 ML QW state of figure 21. However, the presence of the d-band crossing of the Fermi level in the vanadium substrate will suppress the shift in the V Fermi level and thus increase this value.

Note that the systematics of the variation in the experimental energy shifts for the different film thicknesses (table 1) are consistent with this model. Specifically, the shifts should be smallest for the QW states with the lowest energy relative to the bottom of the well (i.e. the largest binding energies relative to E_F), and largest for the smallest binding energy QW states. For example, the 4 ML QW state of the Ag/V(100) system is positioned at 1.4 eV binding energy, i.e. 5 eV from the bottom of the sp band. We calculate a shift of 0.9^{-4} eV K^{-1} for this state, which is very close to the experimentally found value. This correlation is seen in table 1 which includes both the thermal shift coefficients and the QW state binding energies.

In the case of the Ag/Fe(100) system the QW states show opposite temperature dependence [87]; with increasing temperature they shift toward the Fermi level, the effect being largest for the states furthest from the Fermi level. The simple model discussed above reproduces this behaviour; the energy of the Fermi level and the thermal expansion coefficient of iron are 11.1 eV and 11.7×10^{-6} K^{-1} [88], respectively, which gives a value of the temperature dependence of the Fermi energy of 26×10^{-5} eV K^{-1}. For the two QW states discussed above, this value leads to shifts toward the Fermi level of 0.63×10^{-4} eV K^{-1} (2 ML) and 0.90×10^{-4} eV K^{-1} (4 ML), respectively. The measured shift of the 19 ML film QW state is 0.8×10^{-4} eV K^{-1} [87] and this model predicts 0.75×10^{-4} eV K^{-1}, in almost perfect agreement.

A further influence of changing temperature on the observed energies of surface and QW states is the temperature dependence of the substrate band gap. Because the location of this band gap determines the phase shift ϕ_C, this shift influences the standing-wave condition for surface states and QW states. This idea was used to explain the temperature dependence of the surface state spectra of the Cu(111), Ag(111) and Au(111) surfaces [83]. It was found that the phase accumulation model quantitatively reproduces the experimentally determined temperature dependence of the surface state peak energies when the proper temperature dependence of the bulk band gap was taken into account. With increasing temperature the bottom of the band gap shifts up in energy and the top of the gap shifts down. On all these surfaces the surface state lies a few tenths of an eV above the bottom of the band gap, and as the temperature increases

and the bottom of the gap shifts up in energy, the surface states suffers a similar upward shift. When applied to the QW states of the Ag/V(100) system this analysis has exactly the same effect, i.e. it predicts that the QW states should shift up in energy with increasing temperature as for the surface states discussed above, but just the opposite to the effect observed. For this QW system, at least, the calculated effect of the film expansion induced by the temperature increase, as discussed in our earlier interpretation, is much larger than this effect on ϕ_C and causes the states to shift in the opposite direction, as observed experimentally and discussed above.

6. Lineshapes and many-body effects in photoemission from quantum wells

Thermal excitations in a solid also influence photoemission spectral lineshapes and intensities. As we have remarked earlier, photoemission from valence states of a solid can only conserve energy and momentum with the aid of recoil momentum from the solid, and this recoil can couple to the vibrational states of the solid. This vibrational coupling is described by the emission or absorption of a phonon in the electron final state. Phonon scattering of this type has two effects. Firstly, the additional momentum provided by the phonon can scatter a photoelectron out of the cone of the detector, leading to an intensity decrease of the direct transition as the temperature increases. Secondly, photoelectrons can be scattered *into* the detector from initial states not accessible by simple direct transitions, leading to an indirect transition contribution to the photoemission lineshape. Of especial interest to us here is the case of a two-dimensionally periodic system, and photoemission along the surface normal from a Shockley surface state or an s–p-derived QW state. These localized states disperse up in energy (typically parabolically) away from $\overline{\Gamma}$ so the process of phonon scattering *into* the detector (indirect transitions) can add spectral intensity on the high kinetic energy side of the resulting (direct transition) spectral peak up to energies corresponding to photoemission from the highest occupied states at the Fermi level, thus affecting the spectral lineshape. Both the phonon scattering out of and into the detector can be calculated using a simple model based on the Debye–Waller factor following the formulae [89, 90] used by Matzdorf in [91] to discuss the temperature dependence of photoemission from the Cu(111) surface state. However, it has been shown that these contributions, based on reasonable estimates of the relevant Debye temperature, cannot account for the observed degree of peak broadening caused by increased temperature, neither in the case of surface states [91] nor QW states. Consider, for example, the data shown in figure 21 for the case of photoemission from the QW state of the 2 ML Ag film on V(100). The experimentally determined temperature-dependent intensity change of the spectra can be described by an effective Debye temperature of 50 K, but this is a factor of 4.5 smaller than the bulk value and is 2.5 times smaller than the surface value [92]. A similar problem was found for the case of the Cu(111) surface state [91], the Debye temperature needed to describe the data being much smaller than the bulk and surface values.

A further problem with this simple theory is that, while the width of the Cu(111) surface state photoemission peak was found to increase with increasing temperature, the peak retained its symmetrical Lorentzian lineshape. Any significant contribution of final-state indirect transitions should add an asymmetry on the lower binding energy side of the peak as discussed above. In the case of the photoemission spectra from the QW state in the 2 ML Ag/V(100) system of figure 21 this effect is not visible. Obviously, in neither of the two cases discussed here is the final-state direct and indirect transition model able to explain the observed intensity and lineshape changes caused by the temperature increase.

So far we have discussed photoemission as though it were a simple one-electron probe of the bound states in QW structures. In reality, of course, like all spectroscopies, photoemission involves a transition between a ground state and an excited state, and the decay of the resulting

excitation, the photo-hole, introduces many-body effects which are also necessarily probed by the experiments. In the last few years, there has been growing interest in exploiting this aspect of angle-resolved photoemission to characterize these many-body coupling effects. Of particular interest is the electron–phonon coupling, particularly as this phenomenon is a key aspect of conventional superconductivity, and in the context of the present discussion it is widely recognized that the electronic properties of surfaces and ultra-thin films can be quite different from those of bulk solids of the same materials.

In photoemission the many-body interactions of the electronic system ultimately limit the 'lifetime' and 'coherence length' of the photo-hole excitation. In inverse space this introduces a broadening and shift in energy and momentum of the corresponding spectral function

$$A(k,\omega) \propto \frac{\text{Im}\,\Sigma(k,\omega)}{[\omega - \varepsilon_k - \text{Re}\,\Sigma(k,\omega)]^2 + [\text{Im}\,\Sigma(k,\omega)]^2} \tag{14}$$

via the 'self-energy' term $\Sigma(\boldsymbol{k},\omega)$. Angle-resolved photoemission is particularly suitable for studying many-body interactions in low-dimensional systems because, in the case of quasi-two-dimensional systems, it measures directly the photo-hole spectral function given by equation (14). There have already been several such photoemission studies to quantify many-body effects in metallic surface states or in thin films. In a study of the Mo(110) surface state [93] it was shown that all three interaction terms (electron–electron, electron–phonon and defect scattering) can be deduced from the temperature and binding energy dependence of the photoemission peak width. Other studies on metallic surface states on Cu [82, 94, 95], Be [96–98] and Ga [99] focused on the electron–phonon coupling term alone. The results of these studies indicate that the electron–phonon coupling constant, λ (also known as the mass enhancement factor) for surface states determined in this way can be significantly different from that obtained from bulk transport measurements. For example, the value for the Be(0001) surface state is 3–4 times that found in bulk measurements. The λ value for the intrinsic surface state on clean V(100) ($\lambda_V \approx 1.45$) [81, 100] is similarly almost a factor of 2 larger than the bulk value for V of 0.8 [101]. This surface value for V was derived from the mass enhancement of the surface state (band dispersion) near the Fermi level in the same manner as in the earlier surface state studies of Mo(110) [93] and Be(0001) [97, 98].

Angle-resolved photoemission has also been used to study the electron–phonon coupling in QW states in films sufficiently thick (12–19 ML) for the results to be judged to be characteristic of the bulk metal [87, 102]; in this case, some differences in the values deduced have been attributed to the momentum-resolved character of an angle-resolved photoemission measurement as opposed to a directionally averaged transport measurement. This anisotropy of λ [103] may best be illustrated by a comparison between measurements taken in two different directions in Ag films: a study of the Ag/Fe(100) system [87] gave a λ value of 0.24 along the $\{100\}$ direction while a study [102] of 3–6 nm thick Ag(111) films grown on a Cu(111) substrate reported λ values for various QW states in the range of 0.10 ± 0.02 to 0.13 ± 0.02 along the $\{111\}$ main axes, values slightly lower or equal to the averaged (bulk) value of 0.13 reported by Grimvall [104].

In the above examples the films were thick enough to be expected to exhibit bulk-like λ values. In the case of ultra-thin film QWs one may expect that variations in the degree of QW state localization might significantly influence their properties. Indeed, a study of 1 and 2 ML Na films on a Cu(111) surface revealed a λ value of 0.24 for the 1 ML state and a slightly larger value for the 2 ML state [105, 106]. These values are larger than the theoretically estimated values [104] for both Na (0.16) and Cu (0.15) and, as such, suggest that the phonon-induced lifetime broadening of the photo-hole is larger in these very thin films than in the bulk analogues of either overlayer or substrate. This has been confirmed by a theoretical analysis of this problem [105, 107]. Specifically, in the case of a 1 ML Na layer on a Cu(111) surface [108] it was calculated that the electron–phonon coupling in the interface

and overlayer region dominates the lifetime broadening of the QW state spectrum [107]. The key role of the interface is not surprising in this case as the wavefunction of this QW state is equally extended over the sodium layer and several layers of the substrate [105] (figure 11).

While copper and sodium have similar values of the bulk electron–phonon coupling constant, this is not so in the case of silver and vanadium. A recent study of ultra-thin silver films on the V(100) surface, in the coverage range of 1–8 ML, is therefore of considerable interest. This experiment involved extensive measurements of the temperature dependence of the QW photoemission, potentially providing far more detailed information than the simpler single-temperature method of determining the electron–phonon coupling parameter for the intrinsic surface state on the clean V(100) substrate mentioned above. In particular, the electron–phonon coupling of the QW states can be deduced from the temperature dependence of the spectral widths, assuming only that the system can be fairly described by Fermi liquid theory. Having determined this parameter, other contributions to the spectral width can be separated by a careful analysis [93].

Before describing the results of this investigation, however, we should note that an alternative phenomenological approach to discussing QW photoemission lineshapes has been presented, based on an analogue of optical systems. We have already seen that a multiple-reflection model provides a basis for understanding the character of bound states of a QW and an extension of this idea to assess the lineshape and width of QW spectra is to consider the wells as interferometers filled with an absorptive medium [109]. An electron which enters the interferometer (from the vacuum side, i.e. a time-reversed photoelectron) is multiply reflected prior to being absorbed. Its initial-state wavefunction is therefore modulated by an interference factor [41] which depends on the reflectivity at the boundaries R (which is a product of the individual reflectivities at the film/vacuum and film/substrate interfaces), the total reflection phase change Φ for each round trip, the film thickness d and the electron mean free path l defining the absorption:

$$1/\{1 - R\exp[\mathrm{i}(2kd + \Phi)]\exp(-d/l)\}. \tag{15}$$

Based on this Fabry–Perot model one can calculate the photoemission current, peak positions and lineshapes. Temperature-dependent effects are taken into account through the effective change of the well width. This approach has been described and illustrated in the review of Chiang [41]. While this phenomenological theory allows one to model the experimental data effectively, it does not give any clear insight into the microscopic processes that eventually determine the width and the lineshape of the photoemission spectra of QW states, so we do not consider it further.

We now turn our attention to the analysis of the lineshape of the photoemission spectra from QW states in the Ag/V(100) system. Figure 22 shows the photoemission spectra from 1 and 2 ML films (shown overlaid) recorded at a sample temperature of 60 K. The lineshape of the peak from the QW state is completely determined by the photo-hole self-energy $\Sigma(\boldsymbol{k}, \omega)$. Depending on the rate of change with energy of the imaginary part, the spectrum may be either Lorentzian-like (Im Σ approximately constant), asymmetrical or even (for Im Σ very strongly dependent on energy) 'double-peaked' [96]. In figure 22 the experimental spectra are fitted with the 'Fermi liquid' lineshape: $2\mathrm{Im}\,\Sigma(\omega) = \Gamma_0 + 2\beta\omega^2$. The energy-independent term, Γ_0, represents the sum of impurity (or defect) scattering and phonon scattering terms (the phonon contribution being constant at a specific temperature for all energies studied here) and the quadratic term is the electron–electron scattering contribution. Both peaks in figure 22 are fitted by almost the same electron–electron coupling parameter $\beta \approx 0.04\ \mathrm{eV}^{-1}$, a value significantly larger than in bulk-like silver films [87]. These fits lead to values for the constant term Γ_0 of approximately 150 meV for the 1 ML QW state and 100 meV for the 2 ML QW state. We note, however, that the quality of these fits is not very sensitive to the relative values

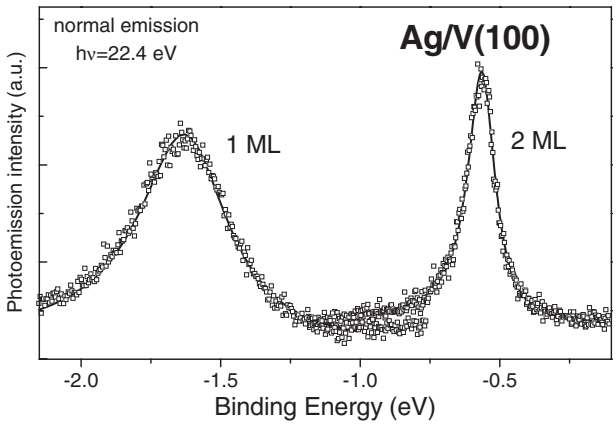

Figure 22. Normal emission photoelectron energy spectra (after linear background subtraction) showing the peaks associated with the QW states in 1 and 2 ML films of Ag on V(100), recorded at 60 K. Both spectra are fitted with the Fermi liquid lineshape (adapted from [100]).

of Γ_0 and β, so this separation of the electron–electron coupling is not very reliable for these data. This is especially true for the 1 ML QW state for which the raw photoemission data clearly show a sloping background, and the exact background used in the analysis evidently influences the degree of asymmetry of the resulting peak.

This ambiguity in separating the various contributions to the peak widths does not, however, extend to the electron–phonon scattering which can be obtained directly from the dependence of the measured photoemission peak widths on temperature; these data are summarized in figure 23. The temperature dependence is approximately linear at high temperatures with a slope of $2\pi\lambda k_B$, where λ is the electron–phonon coupling constant. The linear fits superimposed on the data in figure 23 show that the gradient changes strongly with the film thickness. In figure 24 we plot these experimental λ values deduced from the linear gradients (full circles) as a function of the Ag film thickness d. The most prominent feature of the $\lambda(d)$ plot is the change in the coupling strength of the QW states to phonons when the thickness of the silver film is increased from 1 to 2 ML; the corresponding value of λ for the 2 ML Ag film is more than four times larger than that for the 1 ML QW state ($\lambda_{1\mathrm{ML}} \approx 0.23$, $\lambda_{2\mathrm{ML}} \approx 1.0$) and more than three times larger than the recently reported value measured for a 19 ML Ag film grown on Fe(100), believed to be characteristic of bulk Ag [87]. Apart from the prominent maximum in λ at 2 ML, the Ag/V(100) data of figure 24 show an additional maximum of the coupling constant around 5 ML.

These results have two interesting features: for certain films, very large values of the electron–phonon coupling constant are deduced, and the value of this parameter shows a strong (oscillatory) dependence on film thickness. Of course, changing the film thickness also changes the QW state binding energy in a complex fashion, so the film thickness *per se* may not be the only relevant criterion, as we will discuss below. In the earlier study of the Na/Cu(111) system the electron–phonon coupling of the QW states for the 1 and 2 ML Na films was found to be significantly larger than the bulk coupling constants of both Cu and Na [105, 107], while the coupling constant for the surface state on Cu(111) is essentially identical to that of bulk Cu [82]. These results were taken to imply that the increased electron–phonon coupling strength has its origin in the low dimensionality of the films, rather than in any interaction with the substrate [105, 107]. Similar arguments may not apply to the Ag/V system because the clean V(100) surface state also shows enhanced electron–phonon coupling, as discussed earlier (see also the data point on figure 24).

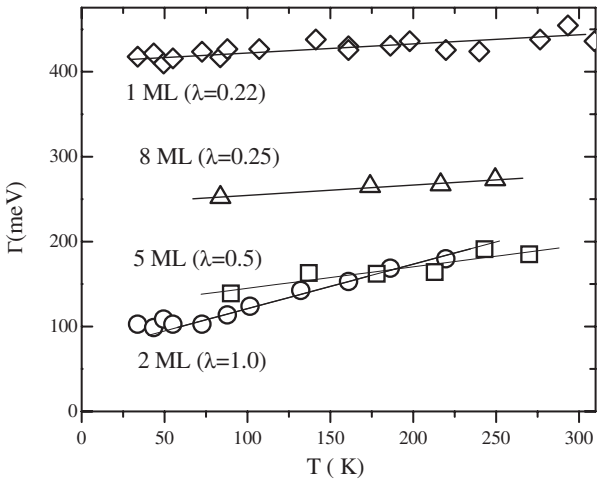

Figure 23. The widths of the photoemission peaks from QW states in Ag films of different thicknesses on V(100) plotted as a function of substrate temperature. Linear fits to each data set are superimposed and these were used to calculate the corresponding electron–phonon coupling constants (λ) which are shown in brackets (adapted from [81, 100]).

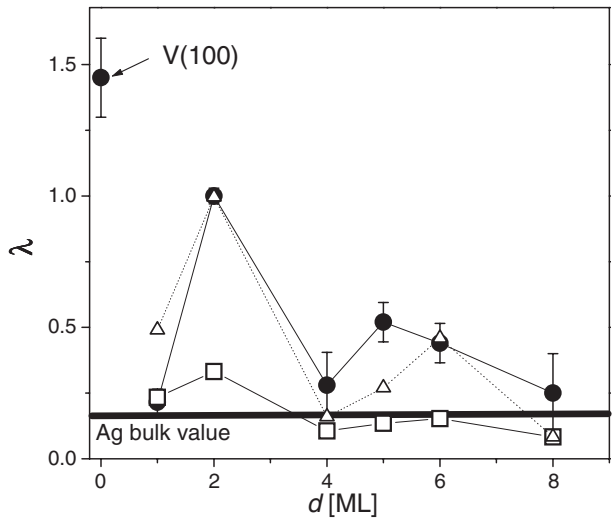

Figure 24. Values of the electron–phonon coupling constant (λ) obtained from photoemission from QW states in Ag films of different thickness (full circles) on V(100) plotted as a function of film thickness. Calculated values of λ, assuming an effective mass $m^* = 1$ for all QWs, are shown as open squares; calculated values including experimentally determined values of the effective mass for each QW state are shown as open triangles. The experimental value of λ for the V(100) surface state is shown at the zero film thickness (from [81]).

In order to understand the origin of the increased and oscillatory thickness-dependent electron–phonon coupling in Ag on V(100) QW states, a simple model was proposed [81, 105] in which the main contribution to the hole lifetime was assumed to be the interaction of the photo-hole with the oscillations of the potential step at the interface between the vacuum and the silver film due to thermal vibrations of the surface atoms. The final formula derived from this theory for the phonon-induced lifetime of the photo-hole created in the QW band i is

$$\frac{1}{\tau} = \frac{A_c}{M\eta^2}\left[\sum_f \left\{ m^f_{xy}\left|T_{fi}\right|^2 (2n(\omega_0)+1)\frac{Y^2(Q_{f,i})}{\omega_0}\right\} + m^i_{xy}\left|T_{ii}\right|^2 (n(\omega_0)+1)\frac{Y^2(Q_{i,i})}{\omega_0}\right] \quad (16)$$

where $Q_{f,i}$ is the wavevector of the phonon emitted (or absorbed) given as

$$Q_{f,i} = \frac{\sqrt{2m^f_{xy}}}{\eta}(E_i(\boldsymbol{K}=0) - E_f(\boldsymbol{K}=0) \pm \eta\omega_0) \quad (17)$$

with $E_i(\boldsymbol{K}=0)$ and $E_f(\boldsymbol{K}=0)$ being the energies of the QW states at the bottom of the ith and fth QW state bands, respectively. A_c is the area of the surface Wigner–Seitz cell, M is the mass of the surface atoms and $n(\omega_0)$ is the Bose–Einstein distribution function.

The key conclusion arising from this model is that, if an electronic state of interest is localized near the surface (and thus has a significant wavefunction amplitude in the region of rapid change in potential at the surface–vacuum interface), and further if there are also final states, similarly localized, to which energy- and momentum-conserving transitions are possible, then one can expect the influence of the surface layer vibrations on the photo-hole lifetime, and consequently on the photoemission lineshape, to be strong. This argument, of course, should also be relevant to intrinsic surface states of clean surfaces and may account for the widely observed electron–phonon coupling enhancement for such states. An extremely similar model was developed independently by Hellsing *et al* [107] to explain the results of the Na/Cu(111) study, and indeed equation (16) above is equivalent to equation (5) of the paper by Hellsing *et al*. The model described by Kralj *et al* [81] is simpler in the parametrization of the interaction matrix elements and does not rely on the results produced by the density functional calculations. It also reproduces the Q dependence of the matrix elements, accounting for the finite size of surface atoms, in a very simple and straightforward fashion. In addition to the experimental values, figure 24 shows theoretical values of the electron–phonon coupling constant derived from the slope of the widths (η/τ) calculated from this theory in the high temperature range. The open squares correspond to values of λ calculated assuming that the effective mass of all the QW states around the centre of the Brillouin zone is equal to one.

These theoretical results reproduce the experimentally observed oscillation of the coupling constant, even if free-electron-like dispersion of all the QW states is assumed. In this case changes in the coupling appear to arise mainly from the different localization of the states, and specifically the amplitude of the associated wavefunctions at the surface barrier. These amplitudes are influenced by the QW state binding energy, the more shallow states extending further into the vacuum, and by the degree of localization as determined by the film thickness, thicker films having more extended states which (when normalized) have lower amplitudes at the surface. The apparently complex (oscillatory) dependence of the electron–phonon coupling with film thickness thus arises from both a direct dependence on the film thickness (localization) but also from the more complex dependence of the QW state energy on film thickness. There is also some influence on the coupling in this simple model associated with differences in the available phase space for the photo-hole decay. In particular, only a single QW state exists in the 1 ML Ag film so only intra-band transitions are possible. For the thicker films both inter- and intra-band transitions can occur. However, calculations allowing only intra-band transitions in all films produce results similar to those shown in figure 24, indicating that this phase space consideration is secondary.

Notice, however, that the above equations contain a dependence on the mean effective electron mass, $m_{x,y}$, of each QW state, and this parameter can be extracted from our experimental determination of the dispersion of the QW state energies around normal emission. As may be seen from these dispersion data presented in figure 25, the electron effective mass varies significantly for different states, and incorporating these values into the theoretical

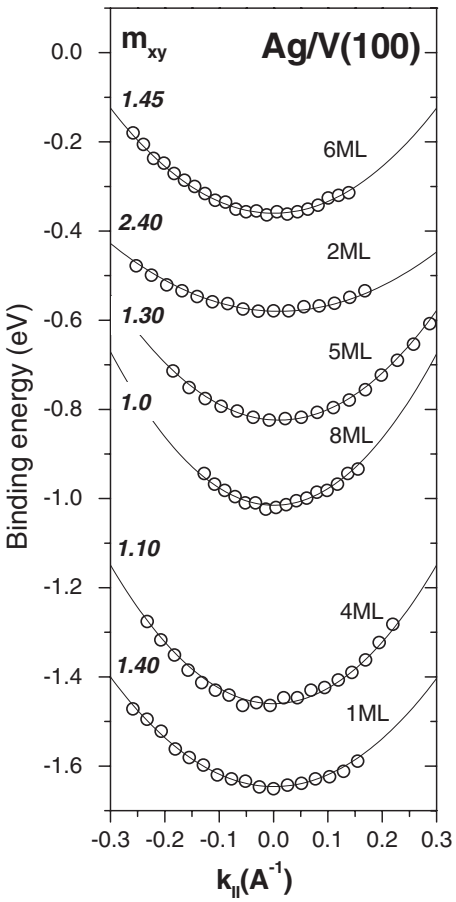

Figure 25. Dispersion of the QW states in Ag films of several thicknesses on V(100), obtained from the angular dependence of the photoemission. Nearly-free-electron parabolic fits to the experimental points give the electron effective mass values shown for each state (adapted from [81]).

calculations gives the open triangles in figure 24. The latter are in significantly better agreement with the experimental λ. The fact that this improvement is so marked, however, is a reflection of the fact that the qualitative character of the variation of electron effective mass with thickness is actually very similar to that of λ in these experiments and in the simple theory. The origin of this $m_{x,y}$ variation is unclear. Large values of $m_{x,y}$ are typically associated with more localized states, and in the past [87] we have argued that the larger values seen in the thinnest films must be related to hybridization of the QW states with the substrate d-bands [110]. This would be favoured for QW states of the highest energies close to the Fermi level, and for the thinnest films, and indeed this correlation is evident in the data of figure 24. Indeed, this correlation is essentially the same as that favouring an important role for the surface phonons in influencing the electron–phonon coupling. Further work, both experimental and theoretical, is clearly warranted to investigate these effects in $m_{x,y}$ more generally, but the experimental results on Ag/V(100) and Na/Cu(111) clearly indicate the importance of the surface phonon coupling for the observed behaviour of λ values.

7. Conclusions

In this review we started from the premise that ultra-thin metal-on-metal films can present QWs which are closely similar to the very simple 'particle-in-a-box' problem which provides the means to introduce students to some of the key consequences of quantum mechanics and

the wave nature of the electron. More detailed consideration, as ever, reveals deeper layers of complexity. The nature of the potential boundaries at the film/vacuum and film/substrate interfaces are more complex than simple 'box walls', but the bound state wavefunctions do retain many of the characteristics of the solutions of a finite rectangular potential well. Exploring the further complications is revealing, and angle-resolved photoemission is a very effective probe of this information.

At its simplest level, photoemission provides a very direct way of measuring the binding energies of the bound QW states, and these energies can be understood in quite a simple way. A key complication relative to the simple rectangular potential well is the influence of the periodic potential within the well introduced by the individual atomic layers, and the role of the truly periodic potential within the substrate to which the QW film states do have some coupling. Angle-resolved photoemission, through its energy and momentum conservation selection rules, provides us with valuable information on this aspect, particularly through the photon energy dependence of the photoemission yield, yet there is conflicting information regarding the role of the atomic potential within the film. For the very thinnest (single monolayer) films, the QW state photoemission behaviour can be expected to be very similar to that of intrinsic (clean surface Shockley) surface states, and there is experimental evidence to support this view. For films of a few atomic layers thickness, the results so far are conflicting. Many studies have been conducted on the Cu(100)/Co(100) fcc film system, and these indicate overlayer atomic periodicity effects may be manifest in films as thin as 3 ML, yet other studies, notably on V(100)/Ag and Cu(111)/alkali metals, indicate quite different phenomena dominate the photon energy dependence of the photoemission yield, pictured in terms of a novel phenomenon of interference between surface and interface photoemission. A key difference here may be the extent to which the substrate and film bulk band structures differ; if they are similar, as in the case of fcc Cu and Co, the distinction between substrate and overlayer atomic periodicity effects may be semantic rather than real.

Most recently, experiments on the temperature dependence of photoemission from metallic QW states, and the closely related clean surface Shockley surface states, have revealed surprisingly strong electron–phonon coupling effects, and complex dependence on film thickness. There are now some simple theories providing an explanation of these effects, yet the size of the experimental database is far too small to be sure that these phenomena are fully understood.

Despite the apparent simplicity of metallic QW systems, and indeed the fact that a quite primitive multiple reflection model is capable of accounting for the energetics, more detailed photoemission experiments in the last few years have revealed a range of phenomena which are still not fully understood, and much further work is required.

Acknowledgments

The authors are pleased to acknowledge the benefit of many fruitful discussions with colleagues and collaborators, and particularly Peter Johnson, Neville Smith, Branko Gumhalter and Tonica Valla. The financial support of The British Council for the Warwick/Zagreb collaboration, and of the Engineering and Physical Sciences Research Council (UK) and the Ministry of Science and Technology (Croatia) grant 00350108 is also gratefully acknowledged.

References

[1] Manoharan H C, Lutz C P and Eigler D M 2000 *Nature* **403** 512
[2] Dascalu D and Rusu A (ed) 2000 *International Semiconductor Conference* 23rd edn CAS 2000 Proceedings (Cat. No 00TH8486) IEEE, Piscataway, NJ, USA
[3] Himpsel F J, Ortega J E, Mankey G J and Willis R F 1998 *Adv. Phys.* **47** 511
[4] Qui Z Q and Smith N V *J. Phys.: Condens. Matter* submitted
[5] Thomas R E 1970 *J. Appl. Phys.* **41** 5330–4

[6] Jaklevic J C, Lambe J, Mikkoe M and Vassell W C 1971 *Phys. Rev. Lett.* 2688
[7] Jaklevic J C and Lambe J 1975 *Phys. Rev.* B **12** 4146
[8] Jalochowski M 1984 *Phys. Status Solidi* a **82** 497–502
[9] Jonker B T, Bartelt N C and Park R L 1982 *Japan Soc. Appl. Phys.* 263
[10] Jonker B T, Bartelt N C and Park R L 1983 *J. Vac. Sci. Technol.* A **1** 1062
[11] Jonker B T and Park R L 1984 *J. Vac. Sci. Technol.* A **2** 813–14
[12] Park R L, Jonker B T, Iwasaki H and Zhu Q-G 1985 *Appl. Surf. Sci.* **22–3** 1
[13] Park R L, Zhu Q-G and Williams E D 1985 *Scanning Electron Microsc.* **4** 1379
[14] Zhu O-G, Yang Y, Williams E D and Park R L 1987 *Phys. Rev. Lett.* **59** 835
[15] Zdyb R, Strozak M and Jalochowski M 1998 *Electron. Technol.* **31** 315
[16] Chauvineau J P and Pariset C 1976 *J. Physique I* **37** 1325
[17] Hoffmann H and Fischer G 1976 *Thin Solid Films* **36** 25
[18] Fischer G and Hoffmann H 1980 *Solid State Commun.* **35** 793
[19] Fischer G, Hoffmann H and Trottmann W 1980 *Vak.-Tech.* **29** 7
[20] Fischer G and Hoffmann H 1980 *Z. Phys.* B **39** 287
[21] Chaudhari P, Habermeier H-U and Maekawa S 1985 *Phys. Rev. Lett.* **55** 430
[22] Jalochowski M and Bauer E 1988 *Phys. Rev.* B **38** 5272
[23] Jalochowski M, Bauer E, Knoppe H and Lilienkamp G 1992 *Phys. Rev.* B **45** 13 607
[24] Jalochowski M, Hoffmann M and Bauer E 1995 *Phys. Rev.* B **51** 7231
[25] Jalochowski M 1995 *Prog. Surf. Sci.* **48** 287
[26] Hinch B J, Koziol C, Toennies J P and Zhang G 1991 *Vacuum* **42** 309
[27] Benedek G, Luo N S, Ruggerone P, Reichmuth A and Toennies J P 1994 *Mater. Sci. Eng.* B **23** 123
[28] Braun J and Toennies J P 1997 *Surf. Sci.* **384** L858
[29] Schmicker D, Hibma T, Edwards K A, Howes P B, MacDonald J E and James M A 1997 *J. Phys.: Condens. Matter* **9** 969
[30] Jalochowski M, Hoffman M and Bauer E 1996 *Phys. Rev. Lett.* **76** 4227
[31] Kirilyuk A, Rasing Th, Megy R and Beauvillain P 1996 *Phys. Rev. Lett.* **77** 4608
[32] Kirilyuk A, Hansen P E, Yuasa S, Katayama T and Rasing Th 1998 *Surf. Sci.* **402–4** 356
[33] Marliere C 1990 *Vacuum* **41** 1192
[34] Villagomez R 1999 *Optik* **110** 299
[35] Xiao M, Villagomez R and Alvarez L 2000 *J. Phys.: Condens. Matter* **12** 2925
[36] Luh D-A, Miller T, Paggel J J, Chou M Y and Chiang T-C 2001 *Science* **292** 1131
[37] Paggel J J, Miller T and Chiang T-C 1999 *Science* **283** 1709
[38] Buergi L, Jeandupeux, Hirstein A, Brune H and Kern K 1998 *Phys. Rev. Lett.* **81** 5370
[39] Echenique P M and Pendry J B 1978 *J. Phys. C: Solid State Phys.* **11** 133
[40] Smith N V and Chen C T 1991 *Surf. Sci.* **247** 133
[41] Chiang T-C 2000 *Surf. Sci. Rep.* **39** 181–236
[42] McRae E G 1979 *Rev. Mod. Phys.* **51** 541
[43] McRae E G and Kane M L 1981 *Surf. Sci.* **108** 435
[44] Smith N V 1985 *Phys. Rev.* B **32** 3549–55
[45] Smith N V and Woodruff D P 1986 *Prog. Surf. Sci.* **21** 295–370
[46] Smith N V, Brookes N B, Chang Y and Johnson P D 1994 *Phys. Rev.* B **49** 332–8
[47] Milun M, Pervan P, Gumhalter B and Woodruff D P 1999 *Phys. Rev.* B **59** 5170–7
[48] Paggel J J, Miller T, Luh D-A and Chiang T-C 2000 *Appl. Surf. Sci.* **162–3** 78
[49] Kawakami R K, Rotenberg E, Choi H J, Escorcia-Aparico E J, Bowen M O, Wolfe J H, Arenholz E, Zhang Z D, Smith N V and Qiu Z Q 1999 *Nature* **398** 132–4
[50] Lindgren I and Walldén L 1988 *Phys. Rev.* B **38** 3060–7
[51] Hufner S 1995 *Photoelectron Spectroscopy: Principles and Applications* (Berlin: Springer)
[52] Kevan S D (ed) 1992 *Angle-resolved Photoemission. Theory and Current Applications* (Amsterdam: Elsevier)
[53] Louie S G, Thiry P, Pinchaux R, Petroff Y, Chandesris D and Lecante J 1980 *Phys. Rev. Lett.* **44** 549–53
[54] Kevan S D, Stoffel N G and Smith N V 1985 *Phys. Rev.* B **31** 1788
[55] Kevan S D, Stoffel N G and Smith N V 1985 *Phys. Rev.* B **31** 3348
[56] Woodruff D P, Milun M and Pervan P 1999 *J. Phys.: Condens. Matter* **11** L105
[57] Henk J and Johansson B 1999 *J. Electron. Spectrosc. Relat. Phenom.* **105** 187
[58] Hansen E D, Miller T and Chiang T-C 1997 *J. Phys.: Condens. Matter* **9** L435
[59] Mugarza A, Ortega J E, Mascaraque A, Michel E G, Altmann K N and Himpsel F J 2000 *Phys. Rev.* B **62** 12 672
[60] Miller T, Hansen E D, McMahon W E and Chiang T-C 1997 *Surf. Sci.* **376** 32

[61] Carlsson A, Claesson D, Lindgren S A and Wallden L 1995 *Phys. Rev.* B **52** 11 144
[62] Carlsson A, Claesson D, Katrich G, Lindgren S A and Wallden L 1996 *Surf. Sci.* **352** 656
[63] Valla T and Milun M 1994 *Surf. Sci.* **315** 81
[64] Valla T, Pervan P and Milun M 1995 *Vacuum* **46** 223
[65] Segovia P, Mascaraque A, Michel E G, Narmann A and Ortega J E 1999 *Surf. Sci.* **433–5** 425
[66] Zhang Z D, Choi H J, Kawakami R K, Escorcia-Aparicio E J, Bowen M O, Wolfe J H, Rotenberg E, Smith N V and Qiu Z Q 2000 *Phys. Rev.* B **61** 76
[67] Kawakami R K, Rotenberg E, Escorcia-Aparicio E J, Choi H J, Wolfe J H, Smith N V and Qiu Z Q 1999 *Phys. Rev. Lett.* **82** 4097
[68] Segovia P, Michel E G and Ortega J E 1996 *Phys. Rev. Lett.* **77** 3455
[69] Altmann N, O'Brien W, Seo D J, Himpsel F J, Ortega J E, Naermann A, Segovia P, Mascaraque A and Michel E G 1999 *J. Electron. Spectrosc. Relat. Phenom.* **101–3** 367
[70] Curti F G, Danese A and Bartynski R A 1998 *Phys. Rev. Lett.* **80** 2213
[71] Ortega J E, Himpsel F J, Mankey G J and Willis R F 1993 *Phys. Rev.* B **47** 1540
[72] Paggel J J, Miller T and Chiang T-C 1999 *J. Electron. Spectrosc. Relat. Phenom.* **101–3** 271
[73] Allen J W 1992 *Synchrotron Radiation Research, Advances in Surface and Interface Science* vol 1, ed R Z Bachrach (New York: Plenum) p 253
[74] Pervan P, Milun M and Woodruff D P 1998 *Phys. Rev. Lett.* **81** 4995
[75] Kaurila T, Vayrynen J and Isokallio M 1997 *J. Phys.: Condens. Matter* **9** 6533
[76] Gallon T E and Matthew J A D 1970 *Phys. Status Solidi* **41** 343
[77] Hagstrum H D 1961 *Phys. Rev.* **123** 758
[78] e.g. Brown D, Crapper M D, Bedwell K H, Butterfield M T, Guilfoyle S J, Malins A E R and Petty M 1997 *J. Phys.: Condens. Matter* **9** 9435
[79] Morris D, Dixon R, Jones F H, Dou Y, Egdell R G, Downes S W and Beamson G 1997 *Phys. Rev.* B **55** 16 083
[80] Zakharov A A, Nylen H, Qvarford M, Lindau I, Leandersson M, Tsetlin M B and Mikheeva M N 1997 *Phys. Rev.* B **56** 9030
[81] Kralj M, Šiber A, Pervan P, Milun M, Valla T, Johnson P D and Woodruff D P 2001 *Phys. Rev.* B **64** 085411
[82] McDougal B A, Balasubramanian T and Jensen E 1995 *Phys. Rev.* B **51** 13 891
[83] Paniago R, Matzdorf R, Meister G and Goldmann A 1995 *Surf. Sci.* **336** 113
[84] Hofmann P, Cai Y Q, Grütter C and Bilgram J H 1998 *Phys. Rev. Lett.* **81** 1670
[85] Citrin P H, Wertheim G K and Baer Y 1977 *Phys. Rev.* B **15** 4256
[86] Valla T, Pervan P, Milun M, Hayden A B and Woodruff D P 1996 *Phys. Rev.* B **54** 11 786
[87] Pagel J J, Miller T and Chiang T-C 1999 *Phys. Rev. Lett.* **83** 1415
[88] Aschroft N W and Mermin N D 1976 *Solid State Physics* (Philadelphia, PA: Saunders)
[89] Pendry J B 1974 *Low Energy Electron Diffraction* (London: Academic)
[90] Shevchik N J 1977 *Phys. Rev.* B **16** 3428
[91] Matzdorf R 1998 *Surf. Sci. Rep.* **30** 153
[92] Harten U, Toennies J P and Woell Ch 1985 *Faraday Discuss. Chem. Soc.* **80** 137
[93] Valla T, Fedorov A V, Johnson P D and Hulbert S L 1999 *Phys. Rev. Lett.* **83** 2085
[94] Matzdorf R, Meister G and Goldmann A 1996 *Phys. Rev.* B **54** 14 807
[95] Theilmann F, Matzdorf R and Goldmann A 1997 *Surf. Sci.* **387** 127
[96] LaShell S, Jensen E and Balasubramanian T 2000 *Phys. Rev.* B **61** 2371
[97] Hengsberger M, Purdie D, Segovia P, Garnier M and Baer Y 1999 *Phys. Rev. Lett.* **83** 592
[98] Balasubramanian T, Jensen E, Wu X L and Hulbert S L 1998 *Phys. Rev.* B **57** R6866
[99] Hofmann P, Cai Y Q, Grütter C and Bilgram J H 1998 *Phys. Rev. Lett.* **81** 1670
[100] Valla T, Kralj M, Siber A, Pervan P, Johnson P D and Woodruff D P 2000 *J. Phys.: Condens. Matter* **12** L477
[101] Brorson S D, Kazeroonian A, Moodera J S, Face D W, Cheng T K, Ippen E P, Dresselhaus M S and Dresselhaus G 1990 *Phys. Rev. Lett.* **64** 2172
[102] Takahashi K, Tanaka A, Sasaki H, Gondo W, Suzuki S and Sato S 1999 *Phys. Rev.* B **60** 8748
[103] Nowak D 1972 *Phys. Rev.* B **6** 3691
[104] Grimvall G 1981 *The Electron–Phonon Interaction in Metals* (New York: North-Holland)
[105] Carlsson A, Lindgren S A, Svenson C and Wallden L 1994 *Phys. Rev.* B **50** 8926
[106] Carlsson A, Hellsing B, Lindgren S-A and Wallden L 1997 *Phys. Rev.* B **56** 1593
[107] Helsing B, Carlsson A, Wallden L and Lindgren S-A 2000 *Phys. Rev.* B **61** 2343
[108] Carlsson J M and Hellsing B 2000 *Phys. Rev.* B **61** 13 973
[109] Himpsel F J 1991 *Phys. Rev.* B **44** 5966
[110] Johnson P D, Garrison K, Dong Q, Smith N V, Li Dongqi J, Mattson J, Pearson J and Bader S D 1994 *Phys. Rev.* B **50** 8954